Biosensors and Bioelectronics 130 (2019) 1–19

Contents lists available at ScienceDirect

Biosensors and Bioelectronics

journal homepage: www.elsevier.com/locate/bios

Aptasensors as a new sensing technology developed for the detection of MUC1 mucin: A review

Meysam Yousefi[a], Sadegh Dehghani[b], Rahim Nosrati[c,d], Hamed Zare[e], Mehdi Evazalipour[f], Jafar Mosafer[g], Bahram Soltani Tehrani[c,h], Alireza Pasdar[a,i], Ahad Mokhtarzadeh[j,k,*], Mohammad Ramezani[l,**]

[a] Department of Medical Genetics, Faculty of Medicine, Mashhad University of Medical Sciences, Mashhad, Iran
[b] Department of Medical Biotechnology, Faculty of Medicine, Mashhad University of Medical Sciences, Mashhad, Iran
[c] Cellular and Molecular Research Center, Faculty of Medicine, Guilan University of Medical Sciences, Rasht, Iran
[d] Department of Pharmaceutical Biotechnology, School of Pharmacy, Mashhad University of Medical Sciences, Mashhad, Iran
[e] Department of Pharmaceutical Biotechnology, School of Pharmacy, Shahid Beheshti University of Medical Sciences, Tehran, Iran
[f] Department of Pharmaceutical Biotechnology, School of Pharmacy, Guilan University of Medical Sciences, Rasht, Iran
[g] Department of Laboratory Sciences, School of Paramedical Sciences, Torbat Heydariyeh University of Medical Sciences, Torbat Heydariyeh, Iran
[h] Department of Pharmacology, School of Pharmacy, Guilan University of Medical Sciences, Rasht, Iran
[i] Division of Applied Medicine, Faculty of Medicine, University of Aberdeen, Foresterhill, Aberdeen AB25 2ZD, UK
[j] Immunology Research Center, Tabriz University of Medical Sciences, Tabriz, Iran
[k] Department of Biotechnology, Higher Education Institute of Rab-Rashid, Tabriz, Iran
[l] Pharmaceutical Research Center, Pharmaceutical Technology Institute, Mashhad University of Medical Sciences, Mashhad, Iran

ARTICLE INFO

Keywords:
MUC1
Mucin
Aptamer
Biosensor
Aptasensor
Cancer biomarker

ABSTRACT

Mucin 1 protein (MUC1) is a membrane-associated glycoprotein overexpressed in the majority of human malignancies and considered as a predominant protein biomarker in cancers. Owing to the crucial role of MUC1 in cancer dissemination and metastasis, detection and quantification of this biomarker is of great importance in clinical diagnostics. Today, there exist a wide variety of strategies for the determination of various types of disease biomarkers, especially MUC1. In this regard, aptamers, as artificial single-stranded DNA or RNA oligonucleotides with catalytic and receptor properties, have drawn lots of attention for the development of biosensing platforms. So far, various sensitivity-enhancement techniques in combination with a broad range of smart nanomaterials have integrated into the design of novel aptamer-based biosensors (aptasensors) to improve detection limit and sensitivity of analyte determination. This review article provides a brief classification and description of the research progresses of aptamer-based biosensors and nanobiosensors for the detection and quantitative determination of MUC1 based on optical and electrochemical platforms.

1. Introduction

Rapid detection and quantification of biomarkers is of paramount importance for diagnosis and clinical management of the human diseases (Florea et al., 2013). For instance, detection of cancer-specific biomarkers in various samples, *e.g.* peripheral blood and serum, has resulted in substantial improvements in early diagnosis of human cancers, as well as monitoring the outcome of the disease during and after the course of treatment (Li et al., 2015; Siegel et al., 2015).

Mucins are a family of high molecular weight, heavily glycosylated proteins produced by epithelial tissues and are classified into two subfamilies: membrane-bound and secreted (gel-forming) mucins; therefore they are an important component in most gel-like secretions, serving functions from lubrication to cell signaling and forming chemical barriers (Marin et al., 2007). Mucin 1 protein (MUC1), as the most studied mucin, is a membrane-associated glycoprotein expressed on the apical surface of most normal epithelial cells (Ma et al., 2013). MUC1 is abnormally overexpressed in the majority of adenocarcinomas and, in particular, in 96.7% of invasive lung cancers (Lakshmanan et al., 2015), 90% of pancreatic, prostate and epithelial ovarian cancers (Roy et al., 2011) and 70% of breast cancers (Rahn et al., 2001), and therefore, has been suggested to be a useful biomarker for the diagnosis

* Corresponding author at: Immunology Research Center, Tabriz University of Medical Sciences, Tabriz, Iran.
** Corresponding author at: Pharmaceutical Research Center, Pharmaceutical Technology Institute, Mashhad University of Medical Sciences, Mashhad, Iran.
E-mail addresses: mokhtarzadehah@tbzmed.ac.ir (A. Mokhtarzadeh), ramezanim@mums.ac.ir (M. Ramezani).

https://doi.org/10.1016/j.bios.2019.01.015
Received 7 October 2018; Received in revised form 31 December 2018; Accepted 4 January 2019
Available online 15 January 2019
0956-5663/

of human cancers, in the early stages (Liu et al., 2015; Yan et al., 2013).

MUC1 consists of a hydrophobic membrane-spanning domain, an extracellular domain at its N-terminal (MUC1-N) and a cytoplasmic domain at its C-terminal (MUC1-C) that are associated with each other *via* hydrogen bonds (Hu et al., 2014). MUC1-N consists of a proline, threonine, and serine (PTS)-rich domain, which is called the variable number tandem repeat (VNTR) region. This region usually contains 12–125 repeats of a 20-amino acids sequence, GSTAPPAHGVTSAPDTRPAP, which is a target for O-glycosylation (Jonckheere and Van Seuningen, 2010). A type of MUC1 which is expressed by cancer cells is usually referred to as tumor-associated MUC1 (TA-MUC1). This protein differs from its normal counterpart in various characteristics. For instance, TA-MUC1 harbors abnormal hypoglycosylation due to decreased activity of b1–6 N-acetyl glucosamine transferase in cancer cells, making novel carbohydrate–peptide antigens such as Thompson–Friedenreich (TF) antigen (bGal(1-3)aGalNAc-O-serine/threonine), Tn antigen (aGalNAcO-serine) and sialyn-Tn (S-Tn a2-6 sialyl GalNAc-O-serine/threonine) (Nath and Mukherjee, 2014; Singh and Bandyopadhyay, 2007). These structural differences have made it possible to design various tests for specific detection of MUC1 and its tumoral counterpart.

A low level of MUC1 expression (generally < 31 U/mL) could be found in healthy human serum (Moreno et al., 2007). However, the normal level of MUC1 in serum may be quite different, depending on the type of assay employed. In cancer antigens detection tests, Cancer Antigen 27–29 (CA 27–29) levels under 40 U/mL (Frenette et al., 1994) and CA 15–3 levels under 25–30 U/mL are usually considered as the levels of MUC1 in normal serum (Rughetti et al., 2008). Thus levels higher than these quantities may usually suggest the presence of malignancies. A 100-fold increase in the amount of MUC1 is indicative of greater likelihood of cancer (Gheybi et al., 2014).

The traditional techniques (including enzyme-linked immunosorbent assay (ELISA), dot blotting, Western blotting, immunohistochemistry, and immunofluorescence) have been applied for the detection of MUC1. Most of these methods are time-consuming, labor-intensive and require expensive instrumentations, limiting their use in real-time clinical diagnostics (Wang et al., 2014; Zhang et al., 2016). Hence, it will be crucial to develop novel methods for sensitive and specific detection of MUC1 in the blood/serum of various human cancers (Yan et al., 2013; Zhao et al., 2015). Among the new and state-of-the-art approaches introduced for the detection of MUC1, biosensor-based methods are becoming consolidated approaches due to their rapid, direct, real-time, efficient and labor-free entity (Ding et al., 2015; Wilson and Gifford, 2005).

Biosensors are compact analytical devices combining a biological recognition element with a transducer which are capable of providing selective quantitative or semi-quantitative sensing of analytes (Turner, 2013). The use of nanomaterials (NMs)/nanoparticles (NPs) in the structure of biosensors can address more sensitive and versatile nano-biosensing platforms with a synergistic performance for the detection of biomarkers (Kong et al., 2011; Mokhtarzadeh et al., 2016). Aptamers have recently been considered as the well-known biorecognition elements for the detection of various analyts including bacteria (Golichenari et al., 2018), natural and chemical material (Eivazzadeh-Keihan et al., 2017; Nosrati et al., 2018) and cancer biomarkers (Dehghani et al., 2018; Eivazzadeh-Keihan et al., 2018; Hasanzadeh et al., 2018), to mention a few. Biosensors which take advantage of these sensitive and selective aptamers are referred to as aptamer-based biosensors, or more concisely, aptasensors.

Aptamers are single-stranded nucleic acids isolated from repeated rounds of an *in vitro* selection called SELEX (systematic evolution of ligands by exponential enrichment) (Bayat et al., 2018; Phillips et al., 2008). Aptamers pose unique characteristics for bioanalytical applications *e.g.* high sensitivity and specificity, target versatility, resistance to degradation and denaturation, cost-effectiveness, ease of synthesis, and stability in non-physiological conditions (Darmostuk et al., 2015; Song et al., 2008). In particular, when interacting with their targets, aptamers undergo a conformational change which abrogates the need for additional labeling alterations for monitoring the binding process (Ogasawara et al., 2009). These unique characteristics suggest aptamers as interesting alternatives to antibodies (Gopinath et al., 2016; Radom et al., 2013). Several MUC1 aptamers have been isolated, including S1.1, S2.2, 5TR1, 5TRG2, MA3, and GalNAc3 (Nabavinia et al., 2017), which have resulted in the development of several types of aptasensors for the detection of MUC1. In this review, we articulate an overview of the recent important achievements in various optical and electrochemical aptasensing platforms for the determination of MUC1, as a main cancer biomarker. Furthermore, we especially emphasize on nanostructured-based aptasensors for the development of highly sensitive and selective MUC1 detection.

2. Optical MUC1 aptasensors and nano-aptasensors

Optical biosensors are becoming increasingly popular with interesting applications in many fields, including healthcare, biomedicine and pharmaceutics and have promising potentials for portable biosensing systems and personalized medicine (Damborský et al., 2016; Fan et al., 2008; Vigneshvar et al., 2016). Optical biosensors recognize the desired analyte with an optical transducer system and take advantage of a biorecognition sensing element which produces a signal proportional to the concentration of the analyte (Damborský et al., 2016). These biosensors have great potentials for real-time and label-free detection of a wide range of substances and benefit from high sensitivity, specificity and cost-effectiveness (Dey and Goswami, 2011; Vigneshvar et al., 2016). In this section, the most prominent examples of optical biosensors and nano-biosensors are described for the detection of MUC1. Tables 1 and 3 show a list of the literatures published for optical MUC1 aptasensors.

2.1. Luminescence-based MUC1 aptasensors and nano-aptasensors

Luminescence is a phenomenon in which light emission does not result from heat (Kulmala and Suomi, 2003). According to the source of energy, various types of luminescence methods are usually classified into a variety of light-emitting processes. For instance, in chemiluminescence (CL), the emission of light is provided by a chemical reaction, whereas electrochemiluminescence (ECL) is the result of an electrochemical reaction in solutions. Luminescence-based methods benefit from high sensitivity and selectivity and large linear quantitative range, and consequently, have become increasingly popular for the development of state-of-the-art analytical techniques (Kulmala and Suomi, 2003; Roda et al., 2016). In this context, several luminescence-based aptasensors for MUC1 detection have been successfully developed (Table 1). Among the chemicals that exhibit CL, ruthenium (Ru) complex and luminol/isoluminol compounds, especially N-(4-aminobutyl)-N-ethylisoluminol (ABEI), have emerged as potent luminophores for the remarkable progress in developing ECL-based MUC1 detection.

The first sensitive strategy for the detection of MUC1 biomarker in breast cancer MCF-7 cells was proposed based on ECL resonance energy transfer (ERET) from ruthenium(II) (Ru1) to graphene oxide (GO) (Wei et al., 2012). RET depends on the energy transfer between two fluorescent molecules - donor and acceptor. ERET systems have shown an excellent potential in analysis and detection fields due to their supersensitivity, high level of controllability, and amplified signal (Z. Li et al., 2017). In this study, Ru1-labeled MUC1 aptamer (Apt_{MUC1}) was used as a probe (Ru1-aptamer complex). In the absence of MUC1, strong noncovalent interactions between Ru1-aptamer and GO, quenched the ECL of Ru1 because of ERET reaction between GO and Ru1. Conversely, upon adding MUC1, the interaction between Ru1-aptamer and GO was disturbed, resulting in the release of Ru1-aptamer from GO and consequently, the restoration of Ru1 ECL (Fig. 1A). This method was shown to detect MUC1 protein in a linear range (LR) from 64.9 nM

Table 1
Comparison of analytical performance of reported luminescence and fluorescence MUC1 aptasensors and nano-aptasensors (nanomaterial-based luminescence and fluorescence MUC1 aptasensors).

Detection method	Strategy/nanomaterial	Recognition motif	Cell/sample	LOD	Linear range	Ref.
Luminescence	Electrochemiluminescence resonance energy transfer (ERET) from bis(2,20 -bipyridine)-(5-aminophenanthroline)ruthenium(II) (Ru1) to graphene oxide (GO)	DNA aptamer	MCF-7	40 nM	64.9–1036.8 nM	(Wei et al., 2012)
	Au-ITO hybrid bipolar electrode amplification system	DNA aptamer	MCF-7	0.5 fM	0.5 fM–1.0 pM	(Wu et al., 2013)
	Cascading amplification of nicking endonuclease-assisted target recycling and rolling circle amplifications	DNA aptamer	Serum	0.71 fg mL^{-1}	10 fg mL^{-1}–10 ng mL^{-1}	(Li et al., 2016)
	Multi-functionalized GO nanocomposite	DNA aptamer	Serum and urine	0.005 ng mL^{-1}	0.005–1000 ng mL^{-1}	(Zhang et al., 2016)
	Photoelectron transfer from CdTe quantum dots to TiO_2 nanotube arrays through DNA chain	DNA aptamer	Serum	0.52 nM	0.002–0.2 μM	(Tian et al., 2016)
	Mercury ion (Hg^{2+}) triggered signal switch coupled with exonuclease I-stimulated target recycling amplification/silver nanoparticles decorated GO nanocomposite/gold nanoparticle	DNA aptamer	Serum	2.6 fg mL^{-1}	10 fg–30 ng mL^{-1}	(Jiang et al., 2016)
	Three-dimensional DNA nanomachine signal probe/catalyzed hairpin assembly (CHA)	DNA aptamer	Serum	0.62 fg mL^{-1}	1 fg mL^{-1}–1 ng mL^{-1}	(Jiang et al., 2017)
	Hollow porous polymeric nanospheres of self-enhanced ruthenium complex	DNA aptamer	Serum	0.31 fg mL^{-1}	1.0–100 pg mL^{-1}	(Chen et al., 2017)
	Dual electrochemiluminescence signal system /luminol-capped gold nanoparticles (Au/luminol) and CdS quantum dots (CdS QDs)	DNA aptamer	MCF-7	20 cells mL^{-1}	100–10^6 cells mL^{-1}	(Zhou et al., 2017)
	Target and mimic target synchronous cycling amplification/DNA nanoflowers	DNA aptamer	buffered solution	0.23 fg mL^{-1}	10^{-3}–10^{-4} pg mL^{-1}	(S.K. Li et al., 2017)
	Enzyme-free target recycling amplification strategy/effective MoS_2 nanoflowers (MoS_2 NFs)-based signal probe/ catalytic hairpin assembly (CHA)	DNA aptamer	Serum	0.58 fg mL^{-1}	1 fg mL^{-1}– 10 ng mL^{-1}	(Li et al., 2018)
	V_2O_5 nanospheres as peroxidase mimics and catalyzed hairpin assembly (CHA) signal amplification	DNA aptamer	Serum	3.33 fg mL^{-1}	10 fg mL^{-1} to 10 ng mL^{-1}	(F. Yang et al., 2018)
Fluorescence	3-Component DNA hybridization system with quantum dot labeling	DNA aptamer	Serum	250 nM	0–2 μM	(Cheng et al., 2009)
	GO as a quencher	DNA aptamer	2% Serum	28 nM	0.04–10 μM	(He et al., 2012)
	Fluorescence resonance energy transfer from quantum dots to GO	DNA aptamer	MCF-7	16 nM	–	(Wei et al., 2012)
	Dual aptamer-modified silica nanoparticles	DNA aptamer	MCF-7 (MUC1 +), SK-BR-3 (HER2 +)	1 cells/100 μL	–	(Jo et al., 2015)
	Target-binding-induced conformation alteration/activatable aptamer probe	DNA aptamer	MCF-7	10 ± 5 cells mL^{-1}	0–10^6 cells mL^{-1}	(Zhao et al., 2015)
	Target-aptamer specific recognition and sensitized luminescence of terbium (III) *via* single strand DNA signal probe/signal-on/label-free	DNA aptamer	MCF-7	70 cells mL^{-1}	500–5 × 10^5 cells mL^{-1}	(Cai et al., 2015)
	Oxidized mesoporous carbon nanospheres (OMCN)	DNA aptamer	MCF-7 (*in vitro* and *in vivo*)	6.52 nmol L^{-1}	0.1–10.6 μmol L^{-1}	(Li et al., 2015)
	Biocompatible carbon dots and GO/fluorescence resonance energy transfer (FRET)	DNA aptamer	Phosphate buffer solution (PBS)	17.1 nM	20–804 nM	(Ding et al., 2015)
	Silicon nanodot (SiND)/ turn-on	DNA aptamer	Serum/MCF-7 (Imaging)	1.52 nM	3.33–250 nM	(Zhang et al., 2018)
	Carbon nanosphere-based fluorescence “turn off/on”	DNA aptamer	MCF-7	25 nM	0–6 μM	(D. Yang et al., 2018)

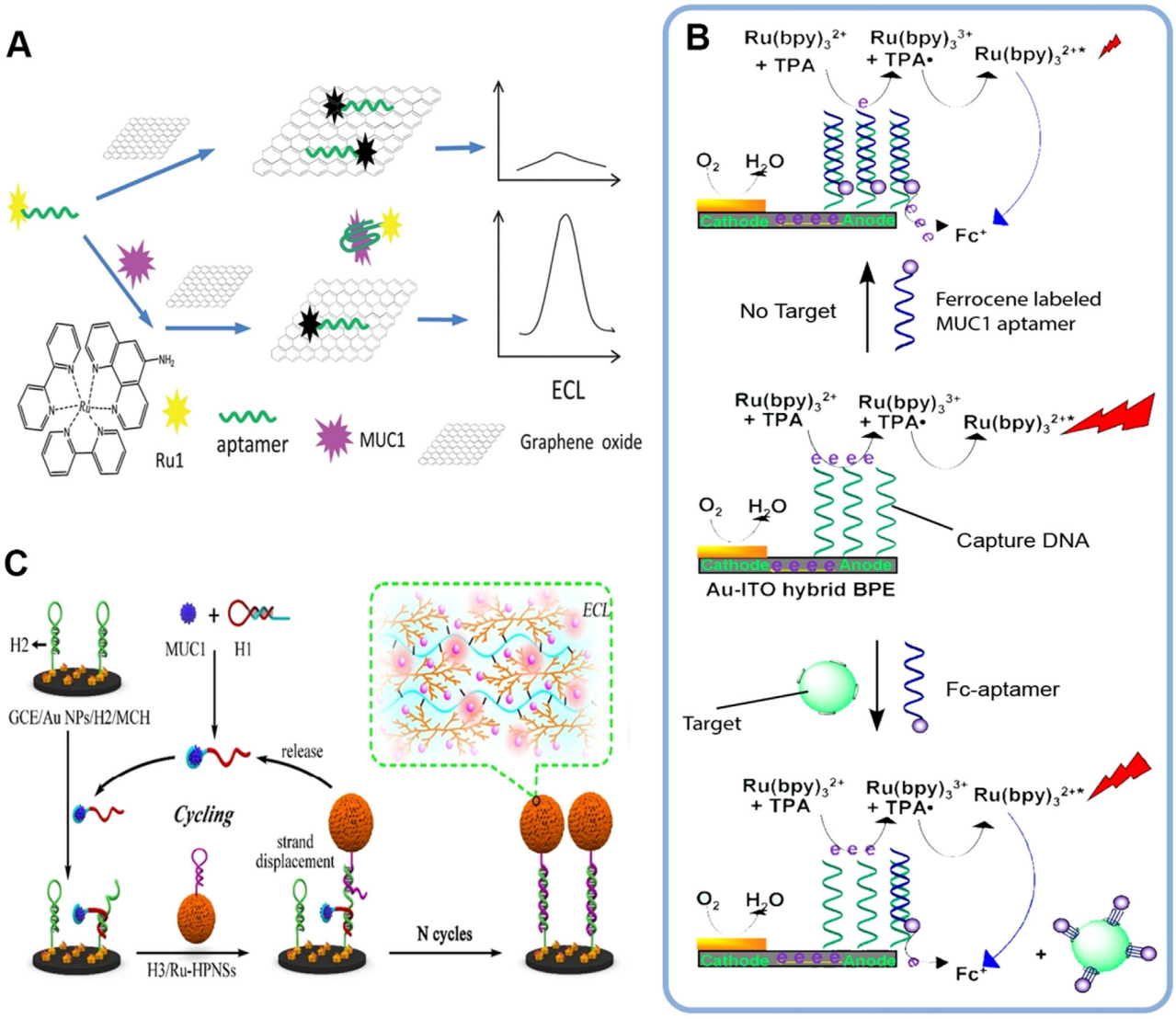

Fig. 1. Schematic illustration of Ruthenium (Ru)-based ECL aptasensors for MUC1 detection. (A) Based on ERET from Ru1 to graphene oxide, reprinted from (Wei et al., 2012) with permission from the Royal Society of Chemistry; (B) A hybrid bipolar electrode (BPE)-ECL biosensor using ferrocene (Fc)-labeled Apt_{MUC1}, reprinted with permission from (Wu et al., 2013), Copyright (2013) American Chemical Society; (C) The hollow porous polymeric nanospheres of a ruthenium complex (Ru-HPNSs) for MUC1 detection. Reproduced with permission from (Chen et al., 2017), Copyright (2017) American Chemical Society.

to 1036.8 nM with a limit of detection (LOD) of 40 nM and MCF-7 cells at concentrations as low as 30 cells mL^{-1}. Another Ru-based ECL for MUC1 detection was a hybrid bipolar electrode (BPE)-ECL biosensor using ferrocene (Fc)-labeled Apt_{MUC1} (Fig. 1B). The BPE-ECL is a microfluidic chip-based ECL system in which an electrode is embedded in a microchannel offering the advantages of low reagent consumption, portability, and disposability. In hybrid BPE, gold nanoparticles (AuNPs) were used as cathode which is able to decrease the over-potential of O_2 reduction while indium tin oxide (ITO) glass was used as the anode to increase the oxidation current of $Ru(bpy)_3^{2+}$/tripropylamine (TPA) on the anode. Without a target, the presence of Fc inhibited the oxidation of $Ru(bpy)_3^{2+}$ and its oxidation form (Fc^+) quenched the ECL of $Ru(bpy)_3^{2+}$/TPA by energy-transfer from the excited-state Ru $(bpy)_3^{2+*}$ to Fc^+. In the presence of MCF-7 cells, Fc-aptamer could interact with MUC1 expressed on the cell surface, resulting in a decreased number of Fc-aptamer hybridized with capture DNA at the anode. This approach allowed detection of Apt_{MUC1} at a concentration down to 0.5 fM and was capable of detecting a minimum of 20 MCF-7 cells mL^{-1}. Besides, the amount of MUC1 on MCF-7 cells was calculated to be 9041 ± 388 molecules/cell (Wu et al., 2013). Recently, an ultrasensitive ECL aptasensor was constructed based on hollow porous polymeric nanospheres of a ruthenium complex (Ru-HPNSs), which is applied as efficient ECL tag, and target-catalyzed hairpin hybridization as signal enhancement strategy for the detection of MUC1 (Fig. 1C). This sensing platform showed a linear response to concentration variations from 1.0 fg mL^{-1} to 100 pg mL^{-1} with the detection limit down to 0.31 fg mL^{-1} (Chen et al., 2017).

Several studies have been carried out based on the quenching effect of ECL emission in ABEI approach. For example; Zhang et al. (2016) reported the development of an ECL aptasensor for the detection of MUC1 using specific binding of this protein to an specific aptamer immobilized on the surface of multi-functionalized magnetic GO nanocomposite ($nanoFe_3O_4$/GO), produced by ABEI. In this system, the role of $NanoFe_3O_4$/GO was to attract the GO nanocomposite on the surface of the magnetic glass carbon electrode (GCE) and thereby enables the ABEI to be immobilized through an increase in conductivity and thus, facilitated the sensitive detection of MUC1. In this study, the authors demonstrated that in the range of 0.005 ng mL^{-1} to 1000 ng mL^{-1}, the ECL intensity diminished linearly relative to the logarithmic concentrations of MUC1. In another study, a multiplex cytosensor was

fabricated based on a dual ECL signal system to detect MCF-7 cells using Au/luminol and CdS QDs as potential-resolved ECL nanoprobes. Human MUC1 aptamer was immobilized onto AuNPs-polyaniline (PANI) on ITO electrodes for capturing MUC1-positive MCF-7 cells. Au/luminol and CdS QDs as ECL nanoprobes were covalently bound to concanavalin A (ConA) and epidermal growth factor (EGF) to label MCF-7 cells on both sides of the sensor, separately. The quantification of MCF-7 cells on two spatially resolved areas was achieved over the linear range from 10^2 to 1.0×10^6 cells mL^{-1} with a detection limit of 20 cells mL^{-1} (Zhou et al., 2017).

In respect to ABEI approach, Ruo Yuan's research group reported numerous studies. In a study, based on quenching effect of mercury ion (Hg^{2+}) on ECL of ABEI, an aptamer-based ECL sensor was fabricated for ultrasensitive determination of Hg^{2+} and MUC1. Concretely, the ECL intensity of GO-AgNPs-ABEI was initially enhanced by ferrocene-labeled single-stranded DNA (ssDNA) (Fc-S1) (first signal switch "on" state) in the presence of H_2O_2. With the aid of aptamer, assistant ssDNA (S2) and full thymine (T) bases ssDNA (S3) modified AuNPs (AuNPs-S2-S3) were immobilized on the sensing surface through the hybridization reaction. Then, an abundance of Hg^{2+} was successfully captured on the AuNPs-S2-S3 *via* strong and stable T-Hg^{2+}-T interaction which effectively inhibited the ECL reaction of ABEI (signal switch "off" state). Finally, the signal switch "on" state was executed by utilizing MUC1 to bind aptamer, leading to a large decrease of the captured Hg^{2+} on AuNPs-S2-S3 (Jiang et al., 2016). In another study conducted by the same group, a significant ECL signal appeared in the presence of MUC1 (1 ng mL^{-1}) based on catalyzed hairpin assembly (CHA) and luminophore ABEI immobilized on a $CoFe_2O_4$ surface (a three-dimensional DNA nanomachine signal probe composed of $CoFe_2O_4$/Au-S2-HP1-ABEI-HP2) (Jiang et al., 2017). The advantage of this platform was the use of $CoFe_2O_4$ which is more stable than Fe_3O_4 in air, and exhibited superior peroxidase-like activity and improved the ECL intensity of ABEI-H_2O_2 system by catalyzing the decomposition of H_2O_2 to generate reactive hydroxyl radical $OH^{\bullet}$. In addition, due to its large surface area, abundant ABEI was immobilized around the $CoFe_2O_4$ surface with amplified ECL signal output due to the CHA reaction (Jiang et al., 2017). This aptasensor showed a relatively low detection limit (0.62 fg mL^{-1}). In a similar study, an ECL aptasensor was proposed for the detection of MUC1 using V_2O_5 nanospheres as peroxidase mimics (F. Yang et al., 2018). In this study, MUC1-aptamer binding triggered CHA for signal amplification (Fig. 2). In this approach, V_2O_5 nanospheres were capable to immobilize a large quantity of ABEI-functionalized AgNPs to form Ag-ABEI/V_2O_5 signal probe. Moreover, V_2O_5 nanospheres not only overcame the intrinsic limitations of natural enzymes, but also could well catalyze H_2O_2 decomposition to generate superoxide anion ($O_2^{\bullet}$) for significant enhancement in the ECL intensity of ABEI. The developed system displayed desirable dynamic range from 10 fg mL^{-1} to 10 ng mL^{-1} and the LOD was down to 3.33 fg mL^{-1} (F. Yang et al., 2018). Recently, a sensitive ECL assay of MUC1 detection was developed with the help of target recycling amplification strategy and effective MoS_2 nanoflower (MoS_2 NF)-based signal probe. In this platform, MoS_2 NFs acted as a co-reaction accelerator, which possessed catalytic performance for H_2O_2 decomposition to enhance the luminous intensity of ABEI-H_2O_2 ECL system. The experimental results showed LR of 1 fg mL^{-1} to 10 ng mL^{-1} while the LOD was 0.58 fg mL^{-1} for MUC1 detection (Li et al., 2018).

Tian et al. (2016) investigated a novel strategy for the construction of MUC1 photoelectrochemical aptasensor, based on photoelectron transfer from Cadmium Telluride (CdTe) quantum dots (QDs) to Titanium dioxide nanotube arrays (TiO_2 NTs) *via* DNA chain. In this study, a series of TiO_2 NTs were prepared on Titanium foil which was then electrodeposited with AuNPs decorated with high amounts of Apt_{MUC1} by Au–S bond to elevate the conductivity. The synthesized cDNA/QDs were then adsorbed on TiO_2 NTs through hybridization of cDNA aptamer, resulting in formation of a TiO_2 NT/aptamer/cDNA/QD aptasensor. In the absence of the analyte, under the irradiation of visible light, the TiO_2 NT/aptamer/cDNA/QD aptasensor showed an excellent photocurrent response due to photosensitivity of CdTe QDs and significant conductivity of Au/TiO_2 NTs and DNA chain. It should be noted that the photocurrent response of the synthesized aptasensor was highly dependent on the length of the DNA chain and morphology of TiO_2 NTs. Taken together, this aptasensor exhibited LOD of 0.52 nM and LR of 0.002–0.2 μM which made it applicable for the detection of low quantities of MUC1 in serum samples. An ECL aptasensor was designed for MUC1 in 40-fold-diluted healthy human serum samples based on cascading amplification of nicking endonuclease-assisted target recycling and rolling circle amplifications (RCA), which showed a LOD down to 0.71 fg mL^{-1} and a LR from 10 fg mL^{-1} to 10 ng mL^{-1} (Yazdian-Robati et al., 2016). S.K. Li et al. (2017) developed a sensitive ECL aptasensor consisting of novel ECL signal tag of DNA NFs and a highly efficient target conversion strategy for MUC1 assay, which not only increased the stability for luminophore loading, but also greatly improved the detection sensitivity to 0.23 fg mL^{-1}.

2.2. Fluorescence-based MUC1 aptasensors and nano-aptasensors

Fluorescence is generally a form of luminescence in which the energy is supplied by electromagnetic radiation (Hötzer et al., 2012). Given the high sensitivity, reproducibility, rapid process and non-destructiveness, fluorescence-based detection methods are of utmost optical techniques for the development of various aptasensors (Hötzer et al., 2012; Pickup et al., 2005; Valeur and Berberan-Santos, 2012). In this regard, there are several interesting studies, have tried to apply fluorescence-based methods for the detection of MUC1.

Firstly, a fluorescence resonance energy transfer (FRET)-based aptasensor was reported for MUC1 detection using a 3-components DNA hybridization system with QD-labeling. In this platform, in the presence of MUC1, the FRET phenomenon occurred after hybridization of aptamer with MUC1 because of the close proximity of the quencher and QDs. The detection limit for MUC1 was in the nanomolar (nM) level (Cheng et al., 2009). In another study by He et al. (2012), a highly sensitive and selective fluorescent aptasensor was constructed utilizing GO to quench the fluorescence signal of single stranded dye-labeled Apt_{MUC1}. In the absence of MUC1, the adsorption of the aptamer on GO brings the dye in proximity of the surface of GO, leading to the quenching of the fluorescent dye. However, in the presence of MUC1, the fluorescence is recovered, and consequently, MUC1 can be detected with a detection limit of 28 nM (wide range of 0.04–10 mM). Another platform was developed based on FRET from conjugation of CdTe QDs to GO. Interaction of aptamer with MUC1 weakened the interaction between the aptamer and GO, resulting in the release of CdTe QDs from GO and thus, the recovery of QDs fluorescence. The detection limits of MUC1 and MCF-7 cells were 16 nM and 36 cells mL^{-1}, respectively (Wei et al., 2012). With respect to photobleaching of dual aptamer-modified silica nanoparticles (SiNPs), two types of breast cancer cells, the MUC1(+) and human epidermal growth factor receptor 2 (HER2)(+) cell lines, were simultaneously detected with a detection limit of 1 cell/100 μL (Fig. 3A) (Jo et al., 2015).

Another FRET-based aptasensor for the detection of MUC1 was reported by Zhao et al. (2015) with a LOD of ~10 ± 5 MCF-7 cells mL^{-1} which is triggered by specific-binding-induced conformation alteration of the designed activatable aptamer probe. The activatable aptamer probe consists of specific Apt_{MUC1}, and an extending spacer making the aptamer in hairpin structure to enable the close proximity of quencher at 3′-terminus to fluorophores (FAM) at 5′-terminus of the probe. Prior to interacting with MCF-7 cells, the fluorescence of the probe is quenched due to FRET between the fluorophore and quencher. After interaction events, the fluorescence signal is activated through specific binding of the probe with target protein on the cell surface (Fig. 3B) (Zhao et al., 2015). In another work, a fluorescence "turn off/on" aptasensor was fabricated by FAM-labeled MUC1 aptamer P0 (P0-FAM) adsorbed onto the surface of carbon nanospheres (CNs). Carbon

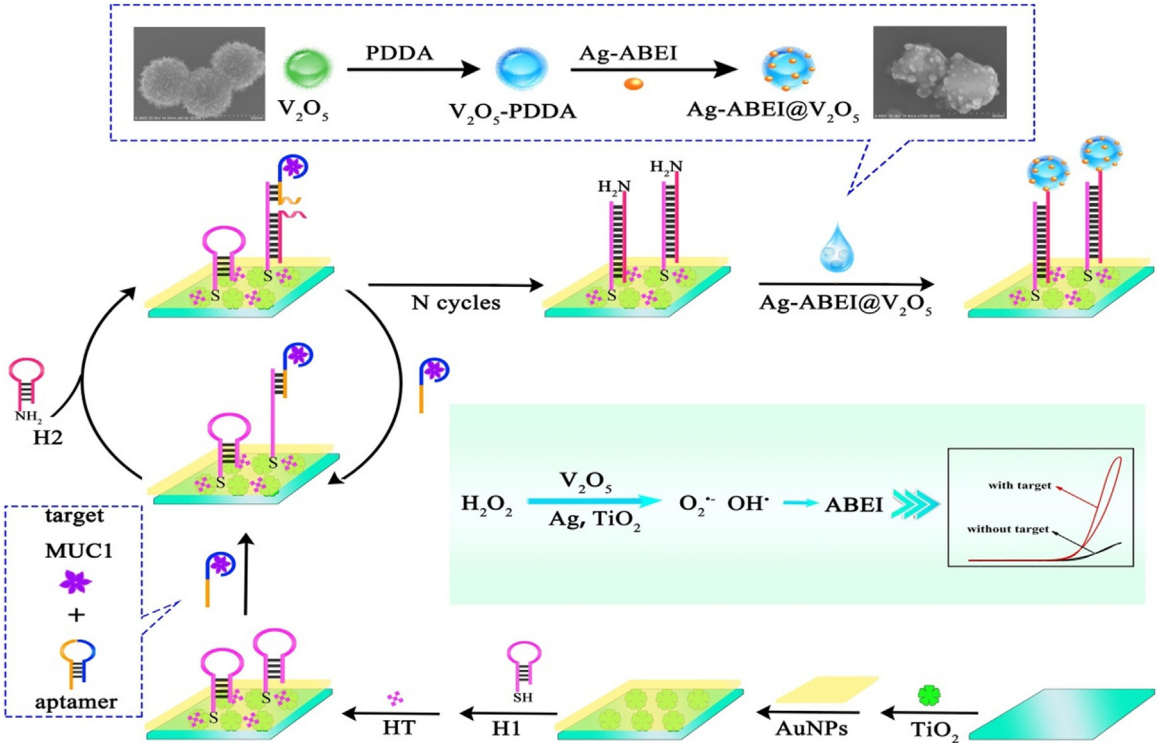

Fig. 2. Schematic representation of an ABEI-based ECL aptasensors for the detection of MUC1. Reprinted with permission from (F. Yang et al. 2018).

nanosphere prepared by the carbonization of glucose had a high fluorescence quenching efficiency (98.8%) while possessed negligible cytotoxicity (in the concentration range of 0–1 mg mL^{-1}, which is 10 folds higher than that of traditional carbon nanotubes or GO (0–100 μg mL^{-1})). As for the detection of the mimic of the tumor antigen MUC1, the resulting fluorescence intensity increased almost linearly in the range of 0–6 μM with LOD of 25 nM (D. Yang et al., 2018).

In an interesting study, Cai et al. (2015) reported that compared to other organic dyes and nanomaterials, the combination of terbium (III) and ssDNA signal probe (Tb^{3+}-SP) is a sensitive probe for the detection of low quantities of MUC1, due to its easy synthesis, stable optical property and suitable biocompatibility. They demonstrated the detection limit of as low as 70 cells mL^{-1}. Li et al. (2015) utilized a Cy3-labeled ssDNA probe (P0-Cy3) *via* "pi stacking" on the surface of oxidized mesoporous carbon nanospheres (OMCN) to achieve fluorescent "turn-on" aptasensor for the detection of MUC1 and cancer cells. This platform detected MUC1 at a detection limit of as low as 6.52 nmol L^{-1} (LR of 0.1–10.6 μmol L^{-1}) and quantified the cancer cells in solution at the detection limit of 8500 cells mL^{-1} (LR of 10^4-2 × 10^6 cells mL^{-1}). They also exploited this OMCN-based aptasensor to image solid tumors such as cells, tissue sections, and *ex vivo* and *in vivo* tumors, with great distinguishability between cancerous and normal tissues. Thus, the multiple diagnosis of cancer *in vitro* and *in vivo* is an advantage of this technique. Ding et al. (2015) reported the development of an ultrasensitive FRET-based aptasensor for the detection of MUC1 based on Apt_{MUC1}-CDs and GO. In this system, the FRET process between CDs and GO was easily achieved due to the efficient self-assembly *via* π–π specific interaction, which resulted in efficient quenching of fluorescence of CDs. Addition of MUC1 resulted in the release of the aptamer–CDs from GO, and the recovery of the fluorescence of CDs as the association constant between aptamer-CDs and MUC1 is bigger than that of aptamer-CDs and GO. This aptasensor was shown to be able to detect MUC1 protein specifically and sensitively in a linear range from 20.0 nM to 804.0 nM with a LOD of 17.1 nM. In another study, a novel dual-color fluorescent aptasensing platform was developed for the detection of MUC1 and visualization of MCF-7 cells *via* fluorescence imaging based on specific interaction of MUC1 and its aptamer, S2.2. This aptasensor was prepared by covalent attachment of the cyanine (Cy5)-tagged aptamer S2.2 to fluorescent silicon nanodot (SiND). In the absence of MUC1, the fluorescence of S2.2-Cy5 was quenched by SiND carrier, whereas in the presence of MUC1, fluorescence was restored due to the structure switching of S2.2. This aptasensor showed specificity for MUC1-positive MCF-7 cells rather than MUC1-negative MCF-10A and Vero cells. The linear range of this method for MUC1 detection was 3.33–250 nM with a LOD down to 1.52 nM (Zhang et al., 2018).

2.2.1. Critical note

According to the obtained data from various developed fluorescence- and luminescence-based MUC1 aptasensors and nano-aptasensors (summarized in Table 1), the ECL-based biosensing platforms are highly sensitive methods showing fg/mL detection limit for MUC1, whereas FRET-based aptasensors allow detecting of MUC1 at the range of nM. Graphene oxide (GO) and QDs have been widely used in FRET-based MUC1 aptasensors due to their great quenching property and other characteristics such as better stability, high spectral resolution and acutely sharp emission bands which could amplify the sensitivity of the platforms (Hasanzadeh et al., 2016; Robertson et al., 1990; Wang et al., 2016). However, the intrinsic fluorescence of some proteins in serum may affect the outcome of the platforms employing GO and QDs and therefore, alter the sensitivity of the sensing platform (Ping et al., 2015). In this regards, it has been reported that pre-treatment of GO with albumin or polyethylene glycol (PEG) (Chung et al., 2013) and using the fluorophores with time-resolved fluorescence properties (Pickup et al., 2005) may help to overcome this limitation as well to diminish the background noises. In addition, inhibition of the GO catalysis reaction caused by transition metal ions, like Zn^{2+} and Fe^{2+} has been reported (Binyamin et al., 2001). The toxicity, chemical instability, low fluorescence signal, multi-exponential decay and photoblinking are also important drawbacks of employing QDs in biosensing methods (Hötzer et al., 2012; Li et al., 2014). However, size-dependent emission is probably the most striking optical property of QDs (Costa-Fernández et al., 2006). The photophysical properties and the

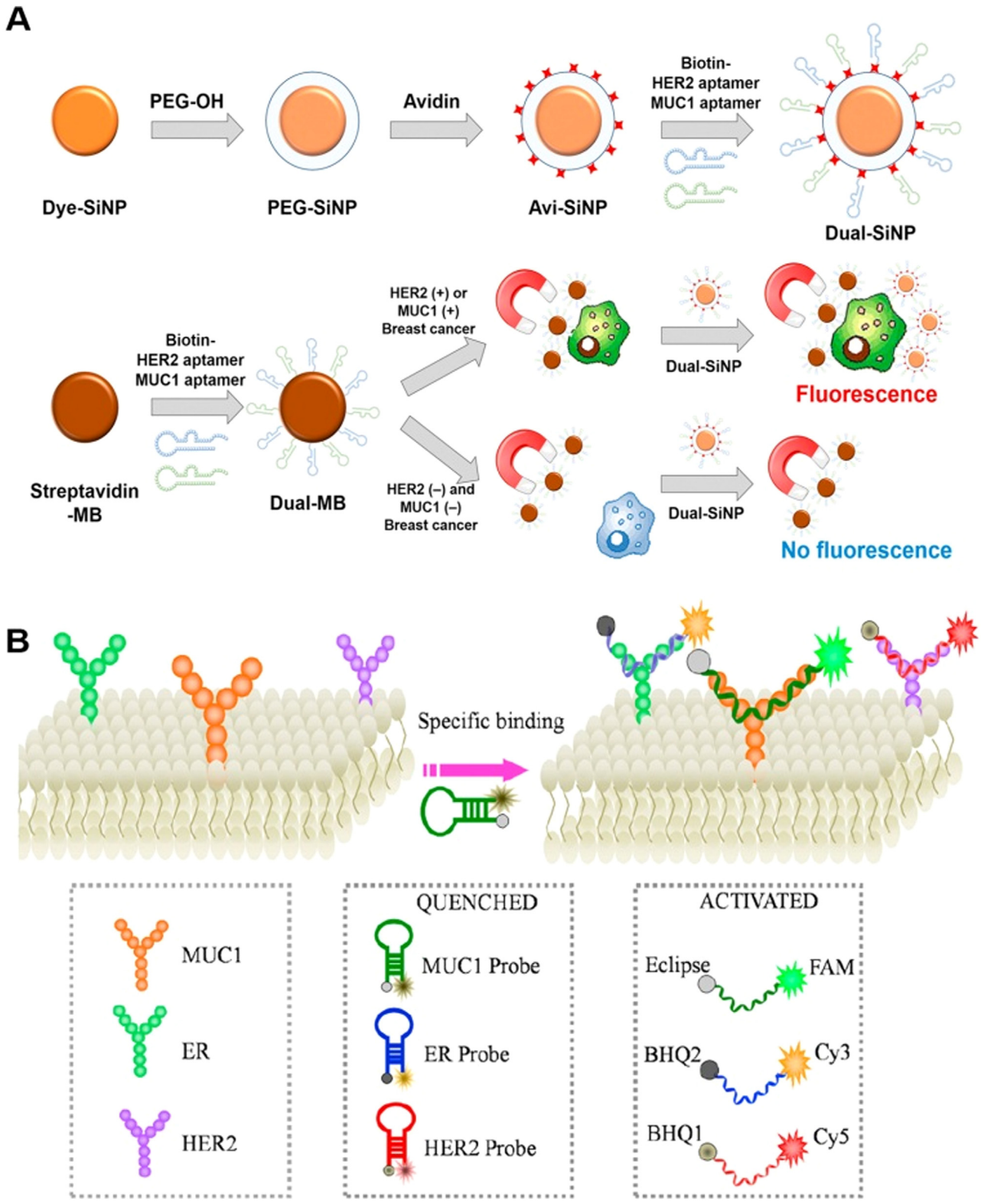

Fig. 3. Schematic of FERT-based aptasensors for the detection of MUC1. (A) Simultaneous detection of HER2(+) and MUC1(+); (B) FAM-labeled MUC1 aptasensors. Reprinted with permission from (Jo et al. 2015; Zhao et al. 2015).

photoactivation of QDs are influenced by many factors, including surface ligand, solvent, temperature, pH and concentration (Sun et al., 2006). Therefore, it should be noted that for an excellent photocurrent response in RET-based systems (ERET and FRET), the optimization of spectra by tuning the size and minimizing the interference between the donor and the acceptor molecules using large surface area, chemical-surface modification and conjugation of a semiconductor nanoparticle with an organic molecule (Costa-Fernández et al., 2006) should be considered.

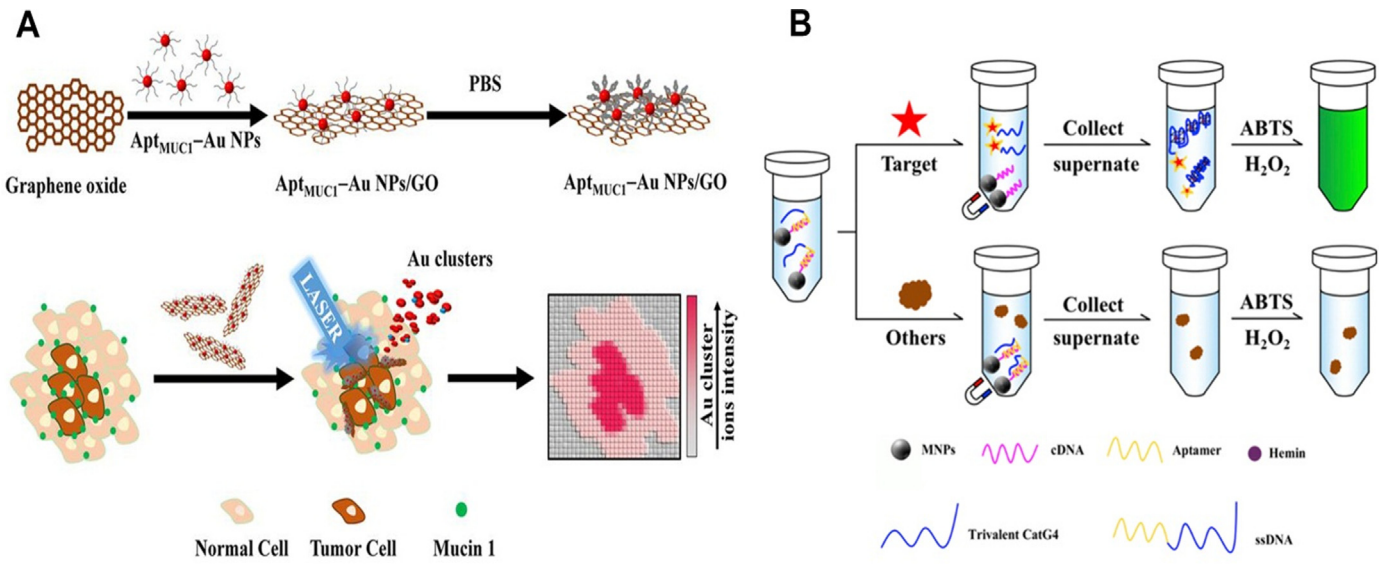

Fig. 4. (A) The sensitive colorimetric aptasensors developed for MUC1 detection. Reprinted with permission from (Huang et al., 2015) under a Creative Commons Attribution 4.0 International License; (B) A label-free colorimetric MUC1 aptasensors. Upon target binding and magnetic separation, the trivalent DNAzyme catalyzed the H_2O_2-mediated oxidation of the ABTS, promoting an obvious colorimetric change visible by the naked eye. Reprinted with permission from (Liu et al., 2018).

2.3. Colorimetric-based MUC1 aptasensors and nano-aptasensors

Colorimetric-based detection systems are one of the most widely applied methods for the detection of biomolecules and analytes (S.K. Li et al., 2017; Su et al., 2011). This detection strategy benefits from a color change, which is easily observed in the presence of target analytes with naked eye with no need for a measuring device (Hutter and Maysinger, 2013; Song et al., 2011).

In a study by Huang et al. (2015), an Apt$_{MUC1}$ was exploited as a targeting agent for nanoparticle-based imaging systems coupled with laser desorption/ionization mass spectrometry (LDI-MS). In this system, the immobilized Apt$_{MUC1}$-AuNPs on GO (Apt$_{MUC1}$-AuNPs/GO) bound effectively to MUC1 units on tumor cell membranes. Then LDI-MS was used to monitor Au cluster ions, resulting in the detection of as few as 100 MCF-7 cells (Fig. 4A). Qi et al. (2016) developed a colorimetric aptasensing system based on oxidase-like activity of MoS_2/PtCu nanocomposites and MUC1 aptamer for the colorimetric detection of various cancer cells with different densities of MUC1. MoS_2 nanosheets could catalyze the oxidation of 3,3,5,5-tetramethylbenzidine (TMB) in the presence of hydrogen peroxide (H_2O_2) to produce a blue color. Liu et al. described the development of a novel label-free colorimetric aptasensor for the sensitive and selective detection of MUC1, which was prepared by coupling of trivalent peroxidase-mimic DNAzyme and magnetic nanoparticles (MNPs) (Fig. 4B). As a trivalent peroxidase-mimic DNAzyme, a three G-quadruplex (G4) DNA-hemin complex was employed, in which hemin could facilitate the G4-DNA to fold into a catalytic conformation and acts as an enzyme. The trivalent DNAzyme catalyzed the H_2O_2-mediated oxidation of ABTS. The colorless ABTS was oxidized and converted into a blue-green product that could be clearly observed and distinguished by the naked eye. The LOD of this system was reported to be down to 5.08–5.60 nM in a LR of 50–1000 nM in a buffer solution and 10% serum system, respectively (Liu et al., 2018).

2.3.1. Critical note

Currently, colorimetric assays are becoming the basis of the available commercial detection kits for MUC1 using antibody-based assays such as ELISA (Table 2). In comparison with available MUC1 detection kits, colorimetric MUC1 aptasensors are currently in the nascent phase, though they show at least equal sensing properties to the commercial MUC1 detection kits. MUC1 nano-aptasensors can be promising tools for point-of-care (POC) in the future of clinical diagnostics because ELISA has a fairly limited detection range and sensitivity compared to developed aptasensors. In addition, antibody-based assays have some restrictions such as requirement of large sample volumes, sophisticated instrumentation, expensive antibodies, long incubation times and complicated protocols (Xu et al., 2017; Zhu et al., 2017). Metal nanoparticles, especially AuNPs can be appropriate candidates for the design of colorimetric MUC1 assays kits owing to the their higher extinction coefficient compared to organic dyes (Devine et al., 1994), which offers high sensitivity for AuNPs-based colorimetric kits. It should be noted that commercial kits have been used for the detection of targets in complex samples like serum. In this line, an important drawback of AuNPs-based kits will be the formation of a dynamic nanoparticle-protein corona named "corona shield effect". The pre-coated AuNPs with specific proteins can solve this problem (Devine et al., 1994).

2.4. SPR/SERs-based MUC1 aptasensors and nano-aptasensors

Surface plasmon resonance (SPR) is a predominant label-free technique for the evaluation of ligand-analyte interactions (Miyazaki et al., 2017). SPR-based sensors, which have gradually become outstanding optical biosensors, sense trivial changes in reflective index with high sensitivity and selectivity, proportional to the mass of biological or chemical species immobilized on the surface of the biosensor (Homola et al., 1999; Wijaya et al., 2011). NPs can enhance the sensitivity of SPR biosensors when applied very close to the SPR substrate and induce significant shifts in the SPR peak position. Currently, SPR biosensors have made great advances in numerous fields, especially in the detection of cancer markers (S.K. Li et al., 2017). Various SPR-based MUC1 aptasensors are discussed in this section and summarized in Table 3.

Sandwich-type SPR aptasensors are a type of SPR-based biosensors utilizing a pair of receptors, which can bind to different sites of the same target and have many advantages including high selectivity, stable and reproducible response and enhanced sensitivity over other platforms (Seo and Gu, 2017). Using MNPs and a two-marker recognition system, a sandwich SPR-based aptasensor was developed for the detection of MCF-7 cells based on the MUC1 detection. While the target MCF-7 cells are captured by Apt$_{MUC1}$, folic acid-conjugated monodisperse MNP is used as the second selective binding reagent to form a sandwich SPR assay with LOD of as low as 500 cells mL^{-1} (Chen et al., 2014). Jia et al. (2016) described another sandwich SPR cytosensor for the detection of MCF-7 cells based on a histidine (His)-tagged

Table 2
Comparison of analytical performance of numerous commercially available MUC1 detection kits.

Commercial MUC1 kit	Assay sensitivity	Assay range	Sample types	Detection method	Assay time
Invitrogen™	4 mU mL^{-1}	4.1–1000 mU mL^{-1}	Supernatants, Plasma, Serum	Colorimetric	4 h 45 min
MyBioSource	0.1 ng mL^{-1}	0.625–20 ng mL^{-1}	Serum, Plasma, Tissue Homogenate, Feces and Urine		Not reported
Cusabio	0.078 mU mL^{-1}	0.312–20 mU mL^{-1}	Serum, plasma, tissue homogenates		1–5 h
Abnova	1 mU mL^{-1}	2.5–50 mU mL^{-1}	Plasma (ACD- or heparinized) and Serum		Not reported
Antibodies-online	0.266 ng mL^{-1}	0.62–40 ng mL^{-1}	Cell Culture Supernatant, Cell Lysate, Tissue Homogenate		3 h
Cloud-clone	0.126 ng mL^{-1}	0.312–20 ng mL^{-1}	Plasma, Serum		3 h

arginine-glycine-aspartic acid (RGD) peptide to link integrin to captured cancer cells. They reported amplification of the SPR signal after binding of NiO-NPs *via* His-tag on the peptide. In this study, MCF-7 cells were captured by the interaction of MUC1 with gold surface modified with Apt_{MUC1}. The use of NiO–RGD can further enhance the SPR response because of the larger mass and higher refractive index of the NiO nanoparticles located in the evanescent field. Implementation of His-tagged RGD, modified by NiO-NPs, was reported to distinguish between MCF-7 cells and normal islet beta cells and exhibited a 20-fold enhancement of DPR signal, resulting in a limit of detection of 136 cells mL^{-1}.

Recently, two-dimensional (2D) zirconium-based metal-organic framework (also described as 521-MOF) nanosheets have been applied for designing of MUC1 aptasensors, due to good electrochemical activity, high surface area (on which large amounts of aptamer strands can be immobilized) and strong affinity interaction between the MOF and the oligonucleotides sequences. This platform, within the concentration range of 0.001 ng mL^{-1} to 0.5 ng mL^{-1} for MUC1 detection in the human serum, exhibited a LOD of as low as 0.12 and 0.65 pg mL^{-1}, deduced from electrochemical impedance spectroscopy (EIS) and SPR, respectively (He et al., 2017). Localized-SPR (LSPR) biosensors have recently drawn much attention for the detection of biomarkers. Compared to SPR, the LSPR systems have the advantages of simpler and more compact set-ups. In a recent study, Apt_{MUC1} and gold nanorods (AuNRs) were utilized to create LSPR platforms which successfully detected the MCF-7 cells by their unique LSPR spectra with a detection limit of 100 cells mL^{-1} (Li et al., 2016).

Surface enhanced Raman spectroscopy (SERS) is a state-of-the-art vibrational spectroscopy which makes it possible to detect low quantities of analytes through the amplification of electromagnetic fields produced during the excitation of localized surface plasmons (Sharma et al., 2012). AuNRs core-silver nanoparticles (AgNPs) satellite assemblies as an ultrasensitive aptamer-based SERS sensor were established for the detection of MUC1 with LOD of 4.3 aM and LR of 0.005–1 fM (Feng et al., 2015). In a study by Qu et al. (2017), self-assembled AuNPs and upconversion nanoparticle (Au–Au–UCNP) trimers were designed based on aptamers to detect MUC1 and alpha-fetoprotein (AFP) as two disease biomarkers. These trimmers created good optical signals with ideal Raman enhancement and quenching effects. The SERS intensity diminished in the presence of MUC1 while it increased in the presence of AFP. With this SERS-encoding sensing system, a limit of detection of 4.1 aM and a wide linear range of 0.01–10 fM for the detection of MUC1 was observed. A paper-based SERS test strip for quantitative detection of MUC1 in whole blood was proposed. On this SERS active substrate, *in situ* synthesized AuNPs stuck to paper fibers in high density, resulting in condensed Raman hot spots. AuNPs were decorated on the paper fibers *via* a CDs assistant strategy, making the strip capable of both sampling and sensing (Fig. 5). This platform was able to detect minute concentrations of MUC1 ranged from 50 ng mL^{-1} to 50 μg mL^{-1} (Hu et al., 2018).

2.4.1. Critical note

The affinity and cross-sensitivity to either mimic or non-target molecules, sample temperature and composition oscillation on the background refractive index can be limited using SPR-based methods for the detection of MUC1 in real and multiplex samples (Frenette et al., 1994). It should be noted that when SPR-based aptasensors are used for the detection of MUC1 in complex samples, the interaction between coexisting biomarkers in samples should be considered. Improvements in specific binding of the MUC1 aptamers to a particular target can overcome this concern.

2.5. Other optical-based MUC1 aptasensors and nano-aptasensors

Aptamer-antibody hybrid sandwich ELISA (Ferreira et al., 2008b), leaky surface acoustic wave (LSAW) aptasensors (Chang et al., 2014), film bulk acoustic resonators (FBARs) and biotin-avidin system /aptamers–AuNP conjugates (Guo et al., 2015) and label-free, fluidic chip by terahertz spectroscopy (Zhao et al., 2017) are used in optical-based MUC1 detection with a slight difference in LOD and linear range, as presented in Table 3.

3. Electrochemical MUC1 aptasensors and nano-aptasensors

An electrochemical aptasensor is a compact analytical device where the bioreceptor (aptamer) is coupled to a transducer surface to convert a biological interaction into a measurable signal (current) that can be easily processed, recorded and displayed (Meirinho et al., 2016). Electrochemical aptasensors, as biosensors, are very attractive for early diagnosis of cancer as these devices are fast, portable, extremely sensitive and selective towards their targets, especially when a bio-recognition element is integrated with the electrode surface (Oguzhan Caglayan, 2017). This section presents sensitive and selective electrochemical aptasensors and nanoaptasensors reported in the literature for specific detection of MUC1 using voltammetric, potentiometric, amperometric and impedimetric techniques (Table 4). To date, several strategies have been used for designing of electrochemical aptasensors for MUC1 detection. A series of platforms have been developed for simultaneous detection of MUC1 and other cancer biomarkers. Other approaches include enzyme-linked sandwich-based electrochemical aptasensors and exonuclease-assisted target recycling amplification. Methylene blue (MB) and $[Ru(NH_3)_6]^{3+}$ have been used as preferred signal transducer in theses platforms.

A sensitive electrochemical immunoassay was reported for the detection of MCF-7 cells according to simultaneous detection of human MUC1 and carcinoembryonic antigen (CEA) on the surface of this cancer cell line (Fig. 6A). The experimental results revealed that this cytosensor can specially monitor MCF-7 cells in a wide range from 10^4 to 10^7 cells mL^{-1} (Li et al., 2010). In another study for the parallel and continuous detection of MUC1 and CEA biomarkers by electrochemical aptasensors based on MB as a signal transducer, the detection limits of MUC1 and CEA were 0.13 nM and 2.75 ng mL^{-1}, respectively. The present biosensing system, after the detection of MUC1, can be continuously used to measure CEA, with the LOD as low as of 0.5 ng mL^{-1} (Liu et al., 2016). Recently, Ma et al. (2018) have reported the development of a dual target electrochemical aptasensor for simultaneous detection of MUC1 and CEA based on $[Ru(NH_3)_6]^{3+}$ electronic wires and metal ion electrochemical labels. In the presence of MUC1 and CEA, the interaction between these biomarkers and their relevant aptamers could lead to the dissociation of double-stranded DNA (dsDNA)

Table 3
Comparison of analytical performance of colorimetric- and SPR/SERS-based MUC1 aptasensors and nano-aptasensors with other optical-based biosensing methods.

Detection method	Strategy/nanomaterial	Recognition motif	Cell/sample	LOD	Linear range	Ref.
Colorimetric	Multivalent aptamer/gold nanoparticle–modified graphene oxide coupled with laser desorption/ionization mass spectrometry (LDI-MS)	DNA aptamer	MCF-7	100 cells	–	(Huang et al., 2015)
	Aptamer conjugated MoS_2/PtCu nanocomposites	DNA aptamer	MCF-7	–	–	(Qi et al., 2016)
	Trivalent peroxidase-mimic DNAzyme and magnetic nanoparticles	DNA aptamer	Buffer solution, 10% Serum	5.08 (buffer solution) 5.60 (10% serum)	50 −1000 nM	(Liu et al., 2018)
SPR/SERS	Label-free/nano-conjugation of monodisperse magnetic nanoparticle and folic acid	DNA aptamer	MCF-7	500 cells mL^{-1}	500 −1 × 10^4 cells mL^{-1}	(Chen et al., 2014)
	NiO nanoparticle-enhanced surface plasmon resonance	DNA aptamer	MCF-7	136 cells mL^{-1}	–	(Jia et al., 2016)
	Two-dimensional zirconium-based metal-organic framework (521-MOF) nanosheets	DNA aptamer	Serum	0.65 pg mL^{-1}	0.001–0.5 ng mL^{-1}	(He et al., 2017)
	Aptamer-functionalized gold nanorods (GNRs)/ localized surface plasmon resonance (LSPR)	DNA aptamer	MCF-7	100 cells mL^{-1}	10^2–10^5 cells mL^{-1}	(Li et al., 2016)
	Active bimetallic gold nanorods (Au NRs) core-silver nanoparticles (Ag NPs) satellite assemblies	DNA aptamer	Serum	4.3 aM	0.005–1 fM	(Feng et al., 2015)
	Self-assembled AuNPs and upconversion nanoparticle (Au–Au–UCNP)	DNA aptamer	Serum	4.1 aM	0.01–10 fM	(Qu et al., 2017)
	Paper-based SERS test strip	DNA aptamer	Human blood	–	–	(Hu et al., 2018)
Other methods	Aptamer–antibody hybrid sandwich ELISA	DNA aptamer	Serum	1 μg mL^{-1}	8–100 μg mL^{-1}	(Ferreira et al., 2008b)
	Label-free/leaky surface acoustic wave (LSAW)	DNA aptamer	MCF-7	32 cells mL^{-1}	10^2–10^7 cells mL^{-1}	(Chang et al., 2014)
	Film bulk acoustic resonators (FBARs) and biotin–avidin system/aptamers–AuNP conjugates	DNA aptamer	PBS	500 nM	30–500 nM	(Guo et al., 2015)
	Label-free/fluidic chip by terahertz spectroscopy	DNA aptamer	PBS and Dulbecco's -PBS solutions	1 pmol mL^{-1}	1–100 pmol mL^{-1}	(Zhao et al., 2017)

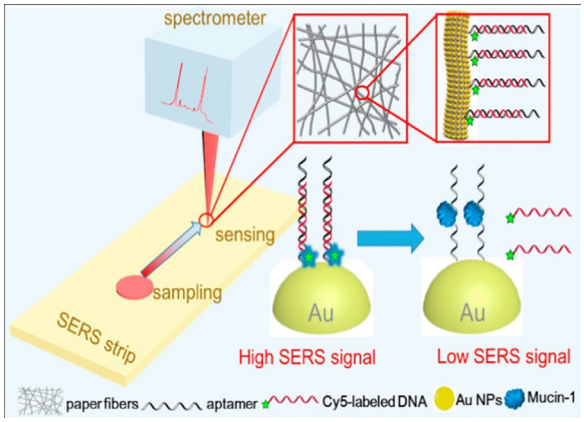

Fig. 5. Scheme of a paper-based SERS test strip for the detection of MUC1. Reprinted with permission from (Hu et al. 2018).

and the analyses of these two targets were realized by DPV peaks produced by metal ion electrochemical labels. To load a large number of metal ions efficiently, Au/bovine serum albumin (Au/BSA) nanospheres were utilized as carriers to prepare Au/BSA-metal ions (Pb^{2+} and Cd^{2+}) which were conjugated with two auxiliary sequences. After embedding of $[Ru(NH_3)_6]^{3+}$ complexes into dsDNA and formation of electronic wires, the electron transfer and electrical conductivity were improved. Consequently, the detection limit of this aptasensing system was calculated as 3.33 fM, ranging from 0.01 pM to 100 nM for MUC1.

Zhao et al. (2012) reported an electrochemical aptasensor, using a ferrocene-labeled aptamer-cDNA as a probe, for the simultaneous detection of MUC1 and vascular endothelial growth factor (VEGF). In this "signal-on" electrochemical biosensing assay, the cDNA immobilized on an electrode surface can be hybridized with both MUC1-specific and VEGF-specific aptamers to form a double strand with ferrocene far away from the electrode surface; hence, electrochemical signal would not be released. However, in the presence of the two protein markers, hybridization of cDNA with aptamers was inhibited and subsequently, the distance between the electrode surface and the ferrocene changed, resulting in an electrochemical signal. This electrochemical signal increased proportional to the addition of either protein markers, but the highest signal was achieved only when both markers were present. In 2013, Ma et al. developed an electrochemical aptasensor for the quantitative detection of MUC1 based on conformational change of electrode-bound Apt_{MUC1} (Ma et al., 2013). The modified electrode was prepared through thiolated MUC1-specific ssDNA aptamers on gold, which were also tethered from the distal end to MB for electrochemical measurements. In the absence of MUC1, the ssDNA aptamers fold into their inherent hairpin conformation, enabling direct electron transfer between MB and gold electrode. Upon addition of MUC1, this protein binds to the ssDNA aptamer, and therefore, the aptamer no longer retains its secondary structure, relocating the redox center (MB) away from the electrode surface. The surface density of DNA aptamer on gold was evaluated by the MB voltammetric response. This response was consistent with that of electrostatically bound $[Ru(NH_3)_6]^{3+}$, demonstrating that each single MB molecule is electroactive at low scan rates and upon binding of MUC1, the electoactivity of MB diminished. The LOD and dynamic response range of this assay were 50 nM and 1.5 μM, respectively, highlighting that this assay is superior to the commercially available ELISA kits.

In a sandwich-based and enzyme-linked electrochemical aptasensor, Apt_{MUC1} is adopted to recognize MCF-7 cells, while enzyme labeling is employed to produce amplified catalytic signals. The molecular recognition and the signal amplification are elaborately integrated by fabricating a sandwich design (Apt_{MUC1}/MCF-7/horse radish peroxidase (HRP)-labeled aptamer) on the gold electrode surface. The detection range can be from 100 to 1 × 10^7 cells, with the detection limit

Table 4
Electrochemical aptasensors for detection of MUC1.

Strategy	Recognition motif	Cell/sample	Limit of detection	Linear range	Ref.
Immunoassay/gold electrode	DNA aptamer	MCF-7	–	10^4–10^7 cell mL^{-1}	(Li et al., 2010)
Signal-on/ferrocene (Fc)-labeled cDNA probe	DNA aptamer	PBS	0.33 nM	1–20 nM	(Zhao et al., 2012)
Immobilization of redox-labeled hairpin DNA aptamers on gold	DNA aptamer	Buffer	50 nM	0–1.5 μM	(Ma et al., 2013)
Aptamer–cell–aptamer sandwich architecture	DNA aptamer	MCF-7	100 cells	100 –1 × 10^7 cells	(Zhu et al., 2013)
p-Aminophenol redox cycling	DNA aptamer	Serum	0.1 nM	0.5–6 nM	(Wang et al., 2014)
Electropolymerization of *o*-aminobenzoic acid (*o*-ABA) onto graphite based screen printed electrodes	DNA aptamer	Buffer	0.62 ppb	1–12 ppb	(Taleat et al., 2014)
Insertion approach/exonuclease-assisted target recycling	DNA aptamer	Buffer	4 pM	10 pM–1 μM	(Wen et al., 2015)
Magnetic beads coupling screen-printed arrays	DNA aptamer	Serum	0.07 nM	0–0.28 nM	(Florea et al., 2015)
Gold electrode- immobilized hybridization assay	DNA aptamer	Serum	0.13 nM	10–100 nM	(Liu et al., 2016)
Self-assembly of a thiolated aptamer tagged with methylene blue/redox label on gold electrodes	DNA aptamer	prostate cancer cells (LNCaP and PC3)	0.65 mL^{-1} (4 nM)	0.65–110 ng mL^{-1}	(Karpik et al., 2017)
Metal ion electrochemical labels/$Ru(NH_3)_6^{3+}$ electronic wires	DNA aptamer	Diluted serum (0.002%)	3.33 fM	0.01 pM–100 nM	(Ma et al., 2018)
Exonuclease I-assisted target recycling amplification	DNA aptamer	Serum	0.40 pg mL^{-1}	1.0 pg mL^{-1}–50 ng mL^{-1}	(Lin et al., 2018)

as low as 100 cells (Zhu et al., 2013). Wang et al. (2014) designed an enzyme-linked electrochemical aptasensor for the detection of MUC1 by *p*-aminophenol redox cycling. Binding of biotinylated MUC1 to streptavidin-alkaline phosphatase led to conjugates which were captured by an anti-Apt_{MUC1}-modified electrode, resulting in the conversion of the *p*-aminophenyl phosphate substrate to the electrochemically active *p*-aminophenol. Subsequent to its oxidization on the electrode, *p*-aminophenol was cycled by Tris phosphine, enabling an increase in the anodic current. Given that MUC1 competed with the conjugate-bound aptamer, the signal diminished proportionally to the elevation of MUC1 concentration between 0.5 and 6 nM, resulting in a LOD of 0.1 nM.

Another electrochemical sandwich aptasensor was developed for MUC1 detection by using MB as an electrochemical indicator and modifying the electrode surface using a functionalized conductive polymer. The primary antibody as the capturing probe was immobilized directly on *o*-aminobenzoic acid (*o*-ABA)-modified electrodes. Then, a sandwich-like structure was fabricated upon MUC1 protein–aptamer complex formation, exploiting aptamer as the detection probe and MB as the electrochemical active marker interacting with the aptamer without previous labeling. Cyclic voltammetry (CV) and differential pulse voltammetry (DPV) were employed to detect changes in MB oxidization peak current which is related to MUC1 concentration. DPV detection revealed a sensitive and reliable detection of MUC1 with LOD of 0.62 ppb and detection range of 1–12 ppb (Taleat et al., 2014). In a later study, two simple and sensitive sandwich electrochemical approaches were developed for MUC1 using magnetic beads coupling screen-printed arrays. In this bioassay, aptamers were coupled respectively to either streptavidin or protein G-modified magnetic beads. The bioreceptor-modified beads were utilized to capture MUC1 from the sample. The sandwich assay was completed by the addition of a labeled secondary aptamer. The enzyme alkaline phosphatase and its substrate (1-naphthyl phosphate) were then used for the electrochemical detection by DPV. In this assay, the LR from 0 to 0.28 nM was obtained with a detection limit of as low as 0.19 nM and 0.07 nM using antibody-based and aptamer-based sandwich assays, respectively (Florea et al., 2015).

Recently, exonuclease (enzyme)-assisted target recycling amplification strategy has been considered in designing of MUC1 electrochemical aptasensors. In this aspect, Wen at al. constructed an electroaptasensor in which the aptamer was labeled with MB and hybridized to capture probe on a gold electrode at both ends to form a dsDNA. Adding MUC1 resulted in the dissociation of the dsDNA and specific recognition and binding of the aptamer to MUC1. Thereafter, exonuclease I (Exo I) was used to digest the aptamer bound to MUC1, and the released MUC1 formed new binding to the remaining aptamer (Fig. 6B). The proposed aptasensor, when properly optimized, had a LR from 10 pM to 1 μM with LOD of 4 pM (Wen et al., 2015). Implementing the same strategy in another study, MUC1 directly released by normal (RWPE-1) and prostate cancer (LNCaP and PC3) cells were detected with a linear detection range of 0.65–110 ng mL^{-1} (Karpik et al., 2017). Unlike the antibody-based immunoassays, the herein described aptasensor did not require handling or processing steps to generate the signal. Another electrochemical aptasensor based on this concept was recently reported. In this study, a DNA bulge-loop (as a L-DNA probe) was fabricated through hybridization of the MUC1 aptamer with cDNA-MB; therefore, due to its electrostatic repulsion, it could not diffuse freely to ITO electrode surface which was negatively charged. Consequently, a small electrochemical signal was detected. Upon addition of MUC1, the L-DNA structure was dissociated because of the specificity between MUC1 and its aptamer. Then, Exo I was implemented to digest the released cDNA-MB into nucleotides which resulted in the production of short MB-labeled mononucleotides fragments (MB-MFs). Given that MB-MFs contained low negative charges, it could easily diffuse to the negatively charged ITO electrode surface and produce a stronger electrochemical signal (Fig. 6C). This enhanced electrochemical signal was linearly proportional to the logarithm of MUC1 concentration in

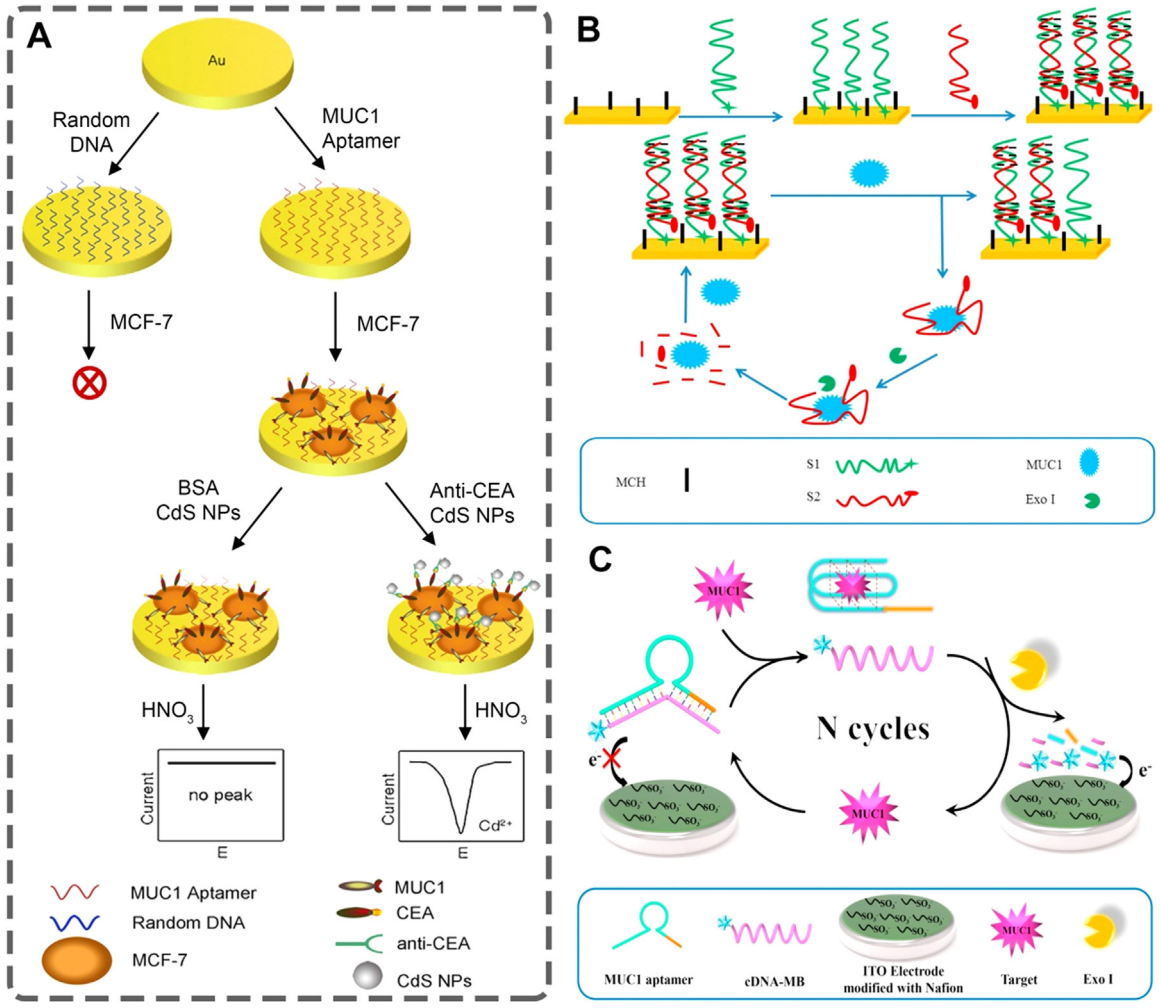

Fig. 6. (A) An immunoassay-based aptasensors for simultaneous detection of MUC1 and carcinoembryonic antigen (CEA); (B and C) The exonuclease I-assisted amplification electrochemical aptasensor for the detection of MUC1. Reprinted with permission from (Li et al. 2010; Wen et al. 2015; Lin et al. 2018).

the range of 1.0 pg mL^{-1}–50 ng mL^{-1} and the LOD for this assay was as low as 0.40 pg mL^{-1} (Lin et al., 2018).

Electrochemical aptasensors combined with NMs are regarded as a versatile platform for cancer markers diagnosis (Croce et al., 2001). NMs increase output signals of electrochemical biosensors by modifying the surface of electrodes and accelerating electron transfer across the electrode and can improve the sensitivity and limit of detection (B. Wang et al., 2017; Zhu et al., 2014). In this platform, metal nanoparticles and carbon-based nanomaterials have received significant attention. In this context, a number of electrochemical MUC1 nano-aptasensors have been developed for the detection of MUC1. A comparison between the LOD and LR of these is summarized in Table 5.

In the first experience, single polypyrrole (PPy) nanowire-based microfluidic aptasensors were fabricated for the detection of MUC1, which showed a very low detection limit of 2.66 nM (Huang et al., 2011). Thereafter, Yan et al. reported the effects of nanoporous materials on the performance of aptasensors for the ultrasensitive electrochemical detection of cancer cells (Yan et al., 2013). In their assay, they used aptamer as a capture probe to bind to MUC1 on the surface of MCF-7 breast cancer cells, forming an aptamer-based sandwich structure for the detection of MCF-7 cells. When functionalized nanoporous materials were integrated into the biosensors, the analytical performance of biosensors was significantly improved by loading large amounts of molecules and accelerating diffusion rate, highlighting the large surface area and versatile porous structure. This aptasensing system showed an excellent analytical performance for the detection of MCF-7 cells ranging from 100 to 5.0 × 10^7 cells mL^{-1} with LOD of 38 cells mL^{-1}.

Two important studies have reported the development of simple electrochemical nano-aptasensors for the detection of MUC1, based on interaction with thiolated aptamers which were immobilized on AuNP-modified graphite and gold SPEs. In the first study, the quantitative detection of MUC1 was carried out by DPV and EIS. LOD of MUC1 for this assay was 0.95 ng mL^{-1} at AuNP-modified gold SPE by DPV methods whereas it was 3.6 ng mL^{-1} at AuNP-modified graphite SPE by EIS (Florea et al., 2013). Another study reported a nanostructured electrochemical aptasensor based on SPEs modified with GO for indirect detection of MUC1. After incubation of MUC1 with its specific aptamer and MB as a redox probe, an electrochemical signal was achieved using DPV and EIS, with a detection limit of 0.6 ng μL^{-1} (Ciui et al., 2016).

Hu et al. (2014) reported a novel nanogold-based aptasensing platform based on a hairpin oligonucleotide (HO) switch, AuNPs and enzyme signal amplification for the detection of MUC1 (Fig. 7A). In their assay, they immobilized HO aptamers and HRP on AuNPs to produce HO–AuNP–HRP conjugates. HRP was also applied as a label for catalyzing the oxidation of *o*-phenylenediamine by H_2O_2 producing 2,3-diaminophenazine (DAP), a reduced product which was detected at the surface of modified electrode and its reduction signal was used as a probe for ultrasensitive detection. Following the recognition between oligonucleotide and MUC1, biotin was exposed and captured by streptavidin onto the surface of the modified electrode. Hence, the

Table 5
Electrochemical nano-aptasensors (nanomaterial-based aptasensors) for the detection of MUC1.

Strategy	Recognition motif	Cell/sample	Limit of detection	Linear range	Ref.
Single polypyrrole (PPy) nanowire-based microfluidic	–	PBS	2.66 nM	–	(Huang et al., 2011)
Porous GO/Au composites and porous PtFe alloy	DNA aptamer	MCF-7	38 cells mL–1	100–5.0 × 10^7 cells mL^{-1}	(Yan et al., 2013)
Electrodeposition of gold nanoparticles on screen printed electrodes	DNA aptamer	Buffer	3.6 ng mL^{-1} (Au NP-modified graphite SPE by EIS) 0.95 ng mL^{-1} (Au NP-modified gold SPE by DPV)	2.5–15 ng mL^{-1} (Au NP-modified graphite SPE by EIS) and 0–10 ng mL^{-1}(Au NP-modified gold SPE by DPV)	(Florea et al., 2013)
Enzyme–gold nanoparticle dual label	DNA aptamer	Serum	2.2 nM	8.8–353.3 nM	(Hu et al., 2014)
Carbon nanospheres/electrochemical impedance spectroscopy (EIS) and cyclic voltammetry (CV)	DNA aptamer	Human colon cancer DLD-1 cells	40 cells mL^{-1}	1.25 × 10^2–1.25 × 10^6 cells mL^{-1}	(Cao et al., 2014)
Electrochemical impedance analysis/gold nanoparticles signal amplification	DNA aptamer	Serum	0.1 nM	0.5–10 nM	(Liu et al., 2015)
Dual signal amplification of poly(*o*-phenylenediamine) –Au nanoparticles hybrid film/AuNPs silica/multi-walled carbon nanotubes core–shell nanocomposites	DNA aptamer	Serum	1 pM	1–100 nM	(Chen et al., 2015)
Covalent immobilization on a conducting polymer nanocomposite	DNA aptamer	MUC1 positive lung cancer cells (A549)	8 cells mL^{-1}	15–1 × 10^6 cells mL^{-1}	(Mir et al., 2015)
GO-modified screen printed electrodes	DNA aptamer	PBS	0.6 ng μL^{-1}	2–20 ng μL^{-1}	(Ciui et al., 2016)
Label-free sandwich polyadenine (polydA)-aptamer modified gold electrode and polydA-aptamer functionalized gold nanoparticles/GO (AuNPs/GO) hybrid	DNA aptamer	MCF-7	8 cells mL^{-1}	10–10^5 cells mL^{-1}	(K. Wang et al., 2017)
Concanavalin A (ConA) on gold nanoparticle	DNA aptamer	MCF-7	500 cells mL^{-1}	5 × 10^2–1 × 10^6 cells mL^{-1}	(Zhang et al., 2017)
Integrated signal probe (ISP)/gold nanoparticles modified glassy carbon electrode (GCE)	DNA aptamer	10 mM phosphate buffer solution	1.06 nM	5 nM–1 μM	(Xiang et al., 2017)
Gold nanoparticles modified glassy carbon electrode	DNA aptamer	Serum	24 nM	50–1000 nM	(Song et al., 2017)
Hierarchical core–shell nanocomposites of zirconium hexacyanoferrate nanoparticles and mesoporous mFe_3O_4/mC(ZrHCF/mFe_3O_4/mC)	DNA aptamer	Serum	0.9 pg mL^{-1}	0.01–1000 ng mL^{-1}	(M. Wang et al., 2017)
Semiconducting polymer dots (PS-COOH–co-PFBT Pdots)/rGO-N'1,N'3 dihydroxymalonimidamide nanosheets	DNA aptamer	Serum	0.06 nM	0.1–14.5 nM	(Farzin et al., 2017)
Gold nanoparticles and GO doped poly(3,4- ethylenedioxythiophene) (PEDOT) nanocomposite films	DNA aptamer	Serum	0.031 fM	3.13 aM–31.25 nM	(Gupta et al., 2018)

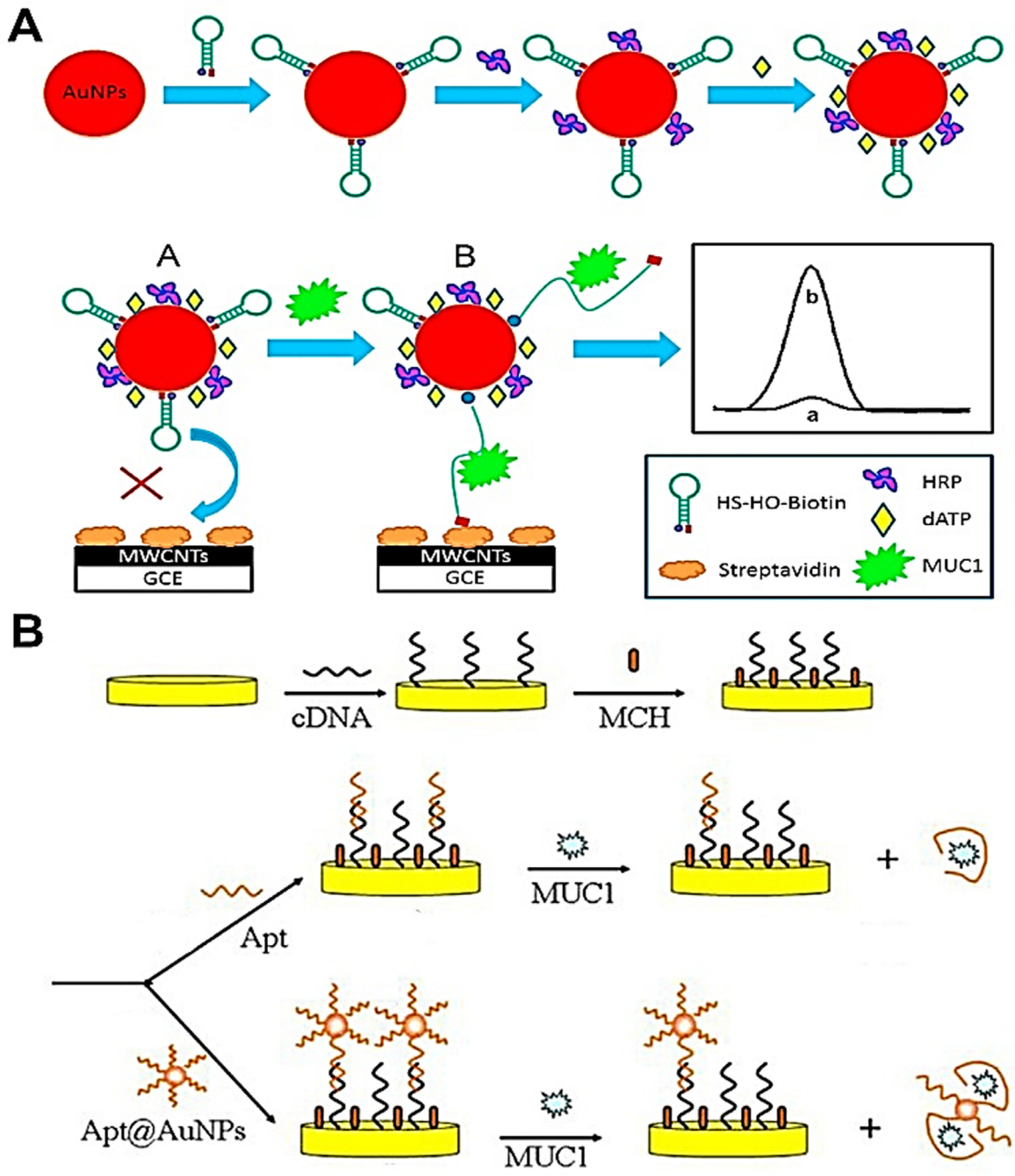

Fig. 7. A nano-aptasensor based on a hairpin oligonucleotide (HO) switch, AuNPs and enzyme signal amplification for the detection of MUC1; (B) An electrochemical impedimetric aptasensor for the determination of MUC1 based on AuNPs signal amplification. Reprinted with permission from (Hu et al. 2014; Liu et al. 2015).

determination of MUC1 could be delicately transduced through detection of the electrochemical reduction signal of DAP. In case of MUC1 detection, this aptasensor had relatively good linear ranges from 8.8 nM to 353.3 nM and LOD of 2.2 nM (Hu et al., 2014). Cao et al. (2014) developed a novel electrochemical aptasensor for quantitative detection of DLD1 colon cancer cells based on the determination of MUC1, which is highly expressed on the surface of this cell line. This aptasensor takes advantage from the interaction between MUC1 and its specific aptamer bound on carbon nanospheres. As sensing layer, these carbon nanospheres (CNs) also accelerated electron transfer and provided a considerably stable matrix for conjugation of target MUC1 aptamer, significantly amplifying the electrochemical signals. To access the optimal performance of the as-fabricated aptasensor, EIS and CV were applied. Binding of DLD1 cells onto Apt_{MUC1} immobilized CNs resulted in elevation of EIS responses which was proportional to DLD1 cell concentration ranging from 1.25×10^2 to 1.25×10^6 cells mL^{-1} with a LOD of as low as of 40 cells mL^{-1}. Liu et al. (2015) developed a selective and sensitive electrochemical impedimetric aptasensor for the determination of MUC1 based on AuNPs signal amplification (Fig. 7B). The designed cDNA, which was partly complementary with Apt_{MUC1}, was immobilized on gold electrode. Addition of MUC1 resulted in switching of aptamer structure from DNA/DNA duplex to DNA/target complex. The change of the interfacial feature of the electrode was characterized by EIS with the redox probe $[Fe(CN)_6]^{3-/4-}$. Subsequently, MUC1 was detected through the changes in electron-transfer resistance (ΔRet). In this aptasensor, the aptamer-modified AuNPs (Apt/AuNPs) conjugates, as the signal enhancer, were introduced to the electrode by the hybridization of cDNA with aptamer.

Chen et al. (2015) reported a novel method for the detection of MUC1 in serum based on a sandwich electrochemical aptasensor, which benefited from a dual signal amplification approach: poly (*o*-phenylenediamine)-AuNPs (PoPD-AuNPs) hybrid film as carrier and AuNPs functionalized silica/ multi-walled carbon nanotubes core-shell nanocomposites (AuNPs/SiO2/MWCNTs), as tracing tag. The PoPD–AuNPs film serves as a microenvironment for stabilizing the primary aptamer while AuNPs/SiO2/MWCNTs increases the surface area for immobilizing secondary aptamer and loading large amounts of electrochemical probe, thionine. Upon addition of MUC1, the sandwich recognition reacted on the aptasensor surface and the thionine-AuNPs/SiO2/MWCNTs probes were adsorbed onto the electrode surface to form bio-complex. AuNPs and MWCNTs facilitate electron transfer from thionine to the electrode and therefore, amplify the detection response. In an optimized condition, this aptasensing system showed a dynamic response range over three orders of magnitude with a LOD of 1 pM.

Mir et al. (2015) designed an aptamer-based MUC1 amperometric nanobiosensor for the detection of A549 human non-small-cell lung cancer (NSCLC) cells. The cytosensing was performed using an Apt_{MUC1} probe with a bioconjugate, where the probe was fabricated by the covalent immobilization on a conducting polymer nanocomposite formed through the self-assembly of 4-([2,2':5',2"-terthiophen]-3'-yl) benzoic acid (TTBA) on AuNPs. A bioconjugate composed of hydrazine and aptamer attached on AuNPs was utilized to reveal the amplified detection signal. The A549 cells were analyzed in a quantitative manner using DPV and microscopic strategies based on silver staining cytosensing experiments. This aptasensor was reported to be highly specific for MUC1 positive A549 cells with a LOD of 8 cells mL^{-1} and dynamic range from 15 to 1×10^6 cells mL^{-1}. Gupta et al. (2018) developed an electrochemical aptasensor based on conducting polymer nanocomposite for the detection of MUC1. AuNPs and GO doped poly(3,4-ethylenedioxythiophene) (PEDOT) nanocomposite films were deposited onto the surface of fluorine tin oxide (FTO) glass sheets by electro-polymerization using chronoamperometry technique. MUC1-specific biotinylated aptamer was immobilized onto the AuNPs-GO-PEDOT nanocomposite film *via* biotin-avidin interaction strategy. The developed aptaelectrode was used for the sensing of MUC1 with LOD of about 1 fg mL^{-1} (0.031 fM). The fabricated aptaelectrode was also applied for the determination of MUC1 in spiked human serum samples with 85–93% recovery.

K. Wang et al. (2017) designed a sandwich electrochemical biosensor for the fast and selective detection of MCF-7 cells by DPV technique. This biosensor was based on polyadenine (polydA)-aptamer modified gold electrode and polydA-aptamer functionalized AuNPs/GO hybrid. Given the inherent affinity between gold and multiple consecutive adenines in the polydA sequences, polydA-modified aptamer was preferred to thiol-terminated aptamer for being immobilized on the surface of a gold electrode and AuNPs/GO. Therefore, the label-free MCF-7 could be easily recognized by the polydA-aptamer and self-assembly onto the surface of gold electrode (Fig. 8A). The polydA-aptamer functionalized AuNPs/GO hybrid could further bind to MCF-7 cells to form a sandwich sensing system. In this assay, CV and EIS were used to characterize the surface-modified gold electrode, using $[Fe(CN)_6]^{3-/4-}$ as a redox probe. The LOD for this assay, under optimal conditions, was reported to be as low as 8 cells mL^{-1} with a linear range of 10–10^5 cells mL^{-1}.

Zhang et al. (2017) developed a sensitive electrochemical aptasensor for the detection and quantification of glycan on the cell surfaces by using cell-specific aptamer, and the lectin-functionalized AuNPs, which were used as both a glycan recognition unit and a signal amplification probe. To construct the aptasensor, amine-functionalized Apt_{MUC1} was first covalently conjugated to carboxylated-magnetic beads (MBs) using the succinimide coupling (EDC-NHS) method. According to the specific interaction of aptamer with MUC1 which is highly expressed on the surface of MCF-7 cells, the aptamer-conjugated MBs showed a significant and selective capability for cell capture. In addition, a lectin-based nanoprobe was designed by noncovalent assembly of concanavalin A (ConA) on AuNPs. This nanoprobe harbored both the capability of specific recognition of carbohydrate and the signal amplification based on the gold-promoted reduction of silver ions. This sandwich-type cytosensor revealed an excellent analytical performance for the quantification of cell surface glycan and determination of MCF-7 cells, especially by coupling with electrochemical stripping analysis. In addition, by utilizing ConA-gold nanoprobe catalyzing silver enhancement, it was possible to track glycolytic inhibition in living cells by naked eye.

An integrated signal probe (ISP)/AuNPs-based aptasensor was used for simultaneous detection of MUC1 and CEA. In this multi-analytes detection, two different aptamer probes as signal probe1 (sP1) and signal probe2 (sP2) which labeled with redox tags MB and Fc, were integrated into one unit DNA structure (Fig. 8B). In ISP-based systems, the integrated signal probe in DNA structure can provide completely similar modification condition and an equal stoichiometric ratio between sP1 and sP2. In addition, the cross interference between sP1 and sP2 can be successfully prevented by regulating the complementary position of sP1 and sP2. In this platform, targets binding to aptamer induced DNA structural switching while the electrochemical responses of MB and Fc were used for the simultaneous dual-analyte detection with the detection limit of 1.82 nM for MUC1 (Xiang et al., 2017).

On the basis of the specific recognition of the MUC1 through the thiolated aptamers that went through immobilization onto the GCE modified by AuNPs, an electrochemical aptasensor was designed for quantitative detection of MUC1 using DPV, together with EIS. This system showed dynamic response range of as high as 1.0 μM and a detection limit of as low as 30 nM (Song et al., 2017). A novel nanostructured hierarchical core-shell nanocomposite of zirconium hexacyanoferrate (ZrHCF) and a mesoporous nanomaterial composed of Fe_3O_4 and carbon nanospheres (denoted as ZrHCF/mFe3O4/mC) was prepared and used as a novel platform for an aptasensor to detect MUC1 with high sensitively and selectively. The prepared ZrHCF/mFe_3O_4/mC nanocomposite exhibited a good linear relationship with the logarithm of MUC1 concentration in a broad range of 0.01 ng mL^{-1} to 1.0 μg mL^{-1}, with a low detection limit of 0.90 pg mL^{-1} (M. Wang et al., 2017).

Lastly, a novel sandwich-type electrochemical aptasensor was designed for the ultrasensitive detection of MUC1 based on aptamer-functionalized semiconducting polymer dots (PSCOOH–co-PFBT Pdots) as the biosensing interface. In this work, rGO-N'1, N'3 dihydroxymalonimidamide nanosheets with large surface area, excellent electroconductivity and good adsorption capacity were not only employed as the ideal carriers to immobilize numerous aptamers, but also acted as the sorbent for the accumulation of electroactive thionine (Th). The constructed biosensing interface could specifically capture tumor marker MUC1, leading to assembly of secondary aptamer-functionalized rGO-N'1,N'3-dihydroxymalonimidamide/Th nanohybride. Consequently, an increase in current intensity of the DPV of adsorbed thionine was monitored and found to be linearly proportional with increasing concentration of MUC1 in the range of 0.1–14.5 nM with a LOD of 0.06 nM (Farzin et al., 2017).

3.1. Critical note

In recent years, various types of biomolecules with differential electrode stability and selectivity have been used for the fabrication of MUC1 electrochemical aptasensors. The biomolecules with good accuracy, admissible stability and reproducibility should be used in electrochemical MUC1 aptasensors. Acquired results of electrochemical-based aptasensors and nanosensors for MUC1 detection at ng mL^{-1} to pM levels are well competitive with other methods previously described. ELISA as a common analytical method mostly used in commercial kits for MUC1 determination allows for detecting MUC1 at the range of ng mL^{-1} levels. For instance, CA 15–3 as a commercial ELISA kit for the detection of MUC1, is estimated to detect 800 nM of MUC1

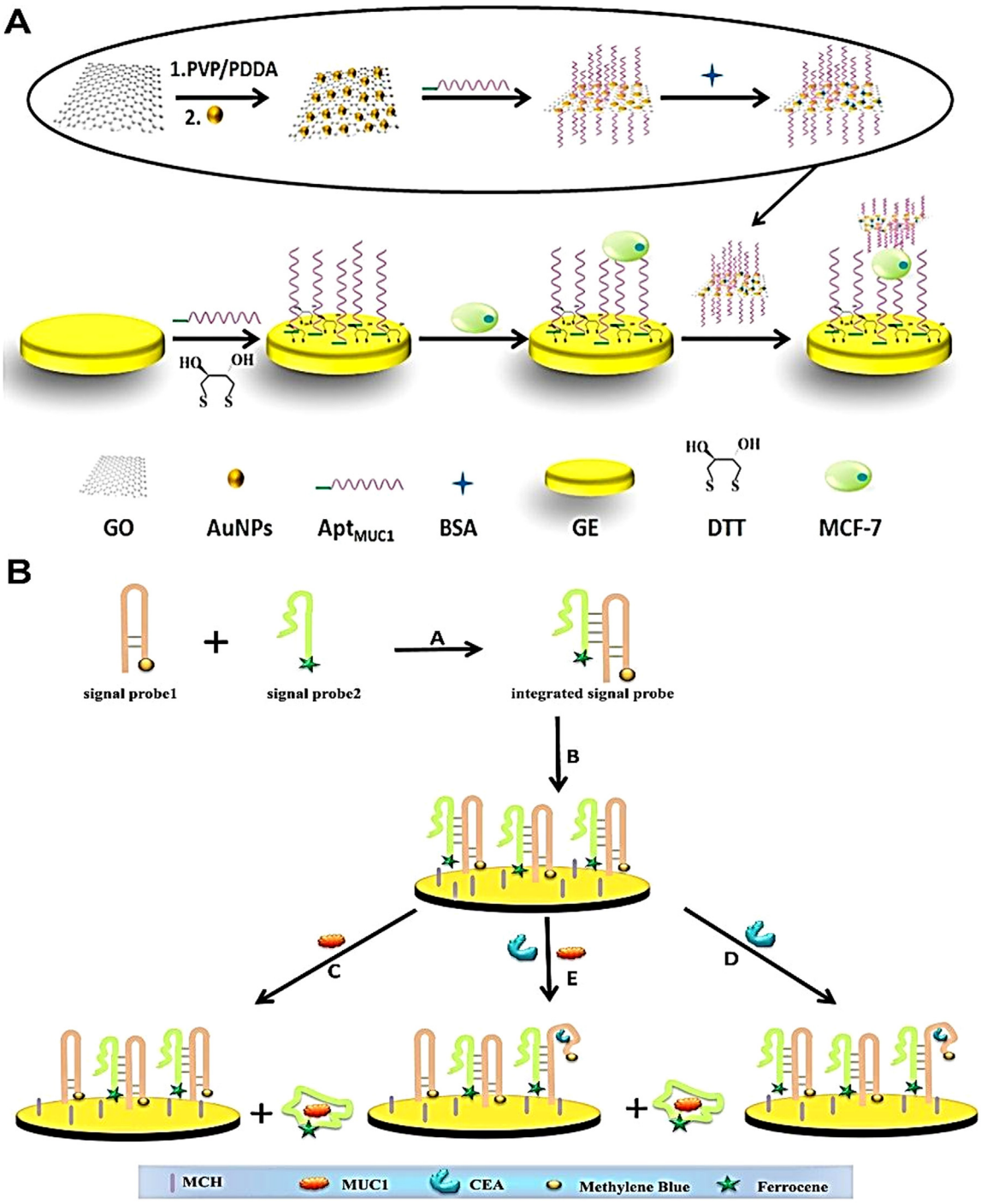

Fig. 8. (A) A sandwich electrochemical biosensor for the detection of MCF-7 cells based on polyadenine (polydA)-aptamer modified gold electrode and polydA-aptamer functionalized AuNPs/GO hybrid; (B) the ISP/AuNPs-based aptasensor for the simultaneous detection of MUC1 and CEA. Reprinted with permission from (K. Wang et al. 2017; Xiang et al. 2017).

(Cheng et al., 2009). However, studies introduced here indicate that the electrochemical-based nano-aptasensors were capable of sensing concentration as low as 0.031 fM to 24 nM of MUC1. As a result, electrochemical-based aptasensors and nanosensors can detect low level of MUC1. This is important considering that MUC1 can be found in blood in trace amounts when cancer is absent while in case of tumor development, its level rises. The detection of low levels of MUC1 is important for the diagnosis, screening and prognosis of cancer in the early stages and also in predicting the outcome of a specific therapy. In comparison with traditional methods, recent methods do not require a pre-concentration step and can measure MUC1 in the nanomolar and sub-nanomolar concentration range.

As an overall critical note, MUC1 can be present in several isoforms: MUC1/TM, MUC1/X, MUC1/Y, MUC1/Z, MUC1/SEC. Moreover, TA-MUC1 has a different structure compared to normal MUC1. The TA-MUC1 has altered glycosylated epitopes recognized by the immune system but it is blocked from antigenic detection in normal MUC1 by large branches of glycosylation (Devine et al., 1993). These properties have been taken into consideration in the design of Apt$_{MUC1}$ and MUC1 aptasensors to discriminate between normal and tumor cells as well as

MUC1 isoforms. In this regard, various anti-MUC1 aptamers have been designed based on different motifs of MUC1 and TA-MUC1-specific antigens such as the murine anti-MUC1 MAb C595 (epitope: Arg-Pro-Ala-Pro) (Missailidis et al., 2005), a highly immunogenic epitope of the VNTR peptide, a long 60-amino acid peptide (Ferreira et al., 2006), the Tn antigen (Ferreira et al., 2008a), the MUC1 tandem repeat (Ferreira et al., 2008a) and APDTRPAPG epitope (Hu et al., 2012). Based on the literature review paper, the S2.2 aptamer with 5'-GCAGTTGATCCTTT GGATACCCTGG-3' sequence has been used more frequently than other anti-MUC1 aptamers for designing aptasensors.

Most studies in which aptasensors were used for the detection of MUC1, have been performed *in vitro*. To date, only few studies suggested that aptamers can be used as targeting agents for imaging of cancer cells. In one such a work, when anti-MUC1 DNA aptamers labeled with QDs were subcutaneously injected into xenograft nude mice, strong fluorescence was observed specifically in the tumor, but not with control QDs (Zhang et al., 2013). An optical-MR-PET imaging technique was also investigated using anti-MUC1 aptamers, which showed high cancer-specific detection in tumor-bearing nude mice (Kang et al., 2015). T. Li et al. (2017) efficiently differentiated MCF-7 cells from more aggressive MDA-MB-231 breast cancer cells and A549 human lung cancer cells based on synthesized aptamer-functionalized Ag nanoclusters conjugated to Apt_{MUC1}. With regards to the potential efficacy of aptamers as targeted radiopharmaceuticals in cancer therapy, Apt_{MUC1} selected against either the protein core (AptA) or the tumor glycosylated (AptB) MUC1 glycoprotein have been conjugated to the ligand MAG2 and labeled with technetium-99 m $^{99\,m}Tc$, for the potential use as radiopharmaceuticals for diagnostic imaging of breast cancer in MCF-7 tumor bearing mice (Da Pieve et al., 2009). In another study, anti-MUC1 nano-aptamers labeled with ^{99m}Tc was used for early diagnosis of MUC1 overexpression in triple-negative breast cancer imaging (TNBC) offering great *in vivo* imaging properties (do Carmo et al., 2017).

There are much needed studies to design aptasensors for the detection of MUC1 *in vivo*, and in complex clinical samples. To the best of our knowledge, no report has been appeared on methods which could be employed in clinic. Interference of designed aptasensors with different biomarkers present in cancer cells remains a challenge to be solved, because more than one biomarker is involved in most of human cancers. Moreover, measurement of local concentrations of the signals secreted by cancer cells *in vivo* is difficult. The optimization of operational conditions such as temperature, pH, ionic strength and buffer components and the immobilization of multiple aptamers on the sensor surface can potentially address the simultaneous detection of several biomarkers in real samples. The fabrication of multiple detection platforms integrated with nanomaterials should be considered for both *in vivo* and complex clinical samples analysis.

4. Conclusions and future perspectives

Nowadays, aptamer-based biosensors have received a great deal of attention for accurate and rapid detection of MUC1 as an important cancer marker. Unique features of aptamers, including ease of synthesis, high sensitivity and specificity and stability in different conditions, have made them interesting choices for developing a wide range of sensing platforms. Another fascinating aspect of utilizing aptasensors is the potential to develop aptasensor arrays for the simultaneous detection of MUC1 and other cancer biomarkers. In this aspect, the improvement of the specific binding of the Apt_{MUC1} to a particular target can overcome this concern.

However, despite various efforts conducted to confirm the efficacy of MUC1 aptamers in various sensing procedures, there is still much effort needed to introduce MUC1 aptasensors as an applicable method for the point-of-care diagnostics. Among several aptamers isolated against MUC1, 5TR1 aptamer has the capability of recognizing mouse PTSMUC1 domain which would increase the chance of being approved by *in vivo* studies followed by entering the preclinical trial phase because *in vivo* tests can be carried out in mouse tumor models instead of using nude mice (Nabavinia et al., 2017). The nuclease degradation, toxicity and limited metabolism of aptamers under physiological environment are suggested as main shortcomings limiting a wider use of aptamers as therapeutics (Keefe et al., 2010; Liu et al., 2017). Thus, in order to decrease the degradation and improve efficiency of aptamer-based therapeutics *in vivo*, chemical modification, remoulding or conjugation with other biomaterials is necessary.

In recent years, the integration of nanomaterials with aptasensing methods has resulted in reasonable improvements in sensitivity and specificity of aptasensors. The rationale behind utilizing nanomaterials in research and in the development of diagnostic systems is that nanomaterials exhibit exceptional functional properties that are often not available from either bulk materials or discrete molecules. For instance, nanomaterials have large surface-to-volume ratio for highly efficient target interactions. This property can be exploited to enhance the performance of traditional methods or develop new assays with ultrasensitivity and multi-parametric capabilities. In this regard, nano-biosensors have reached detection limit ranging from picomolar to attomolar levels, which offer promises for opening a new era of early cancer detection *in vitro* and *in vivo*. However, a general concern with regard to the bio-safety of nanomaterials should be considered for *in vivo* detection of protein markers including MUC1. One final recommendation is to consider the effect of protein corona on the *in vivo* fate of MUC1-targeted NPs. Taken together, given the versatile entity of sensing platforms, drastic advances are expected to happen in the development of MUC1 aptasensors in parallel with on-chip and miniaturized sensing structures such as microfluidic-based aptasensors and nano-aptasensors, with potentially significant applications in clinical diagnostics.

CRediT authorship contribution statement

Meysam Yousefi: Writing - review & editing, Writing - original draft. **Sadegh Dehghani:** Writing - review & editing, Writing - original draft. **Rahim Nosrati:** Conceptualization. **Hamed Zare:** Writing - review & editing. **Mehdi Evazalipour:** Writing - review & editing. **Jafar Mosafer:** Writing - review & editing. **Bahram Soltani Tehrani:** Writing - review & editing. **Alireza Pasdar:** Validation. **Ahad Mokhtarzadeh:** Supervision. **Mohammad Ramezani:** Supervision.

Acknowledgments

This study was financially supported by grant No. 960604 of the Biotechnology Development Council of the Islamic Republic of Iran.

Conflict of interest

The authors declare that they have no conflict of interest.

Declaration of interests

None.

References

Bayat, P., Nosrati, R., Alibolandi, M., Rafatpanah, H., Abnous, K., Khedri, M., Ramezani, M., 2018. Biochimie 154, 132–155.
Binyamin, G., Chen, T., Heller, A., 2001. J. Electroanal. Chem. 500 (1–2), 604–611.
Cai, S., Li, G., Zhang, X., Xia, Y., Chen, M., Wu, D., Chen, Q., Zhang, J., Chen, J., 2015. Talanta 138, 225–230.
Cao, H., Ye, D., Zhao, Q., Luo, J., Zhang, S., Kong, J., 2014. Analyst 139 (19), 4917–4923.
Chang, K., Pi, Y., Lu, W., Wang, F., Pan, F., Li, F., Jia, S., Shi, J., Deng, S., Chen, M., 2014. Biosens. Bioelectron. 60, 318–324.
Chen, A., Zhao, M., Zhuo, Y., Chai, Y., Yuan, R., 2017. Anal. Chem. 89 (17), 9232–9238.
Chen, H., Hou, Y., Ye, Z., Wang, H., Koh, K., Shen, Z., Shu, Y., 2014. Sens. Actuator B-Chem. 201, 433–438.

Chen, X., Zhang, Q., Qian, C., Hao, N., Xu, L., Yao, C., 2015. Biosens. Bioelectron. 64, 485–492.
Cheng, A.K.H., Su, H., Wang, Y.A., Yu, H.-Z., 2009. Anal. Chem. 81 (15), 6130–6139.
Chung, C., Kim, Y.-K., Shin, D., Ryoo, S.-R., Hong, B.H., Min, D.-H., 2013. Acc. Chem. Res 46 (10), 2211–2224.
Ciui, B., Tertiş, M., Peia, D., Cristea, C., Săndulescu, R., 2016. Farmacia 64 (1), 43–47.
Costa-Fernández, J.M., Pereiro, R., Sanz-Medel, A., 2006. TrAC Trends Anal. Chem. 25 (3), 207–218.
Croce, M.V., Isla-Larrain, M.T., Price, M.R., Segal-Eiras, A., 2001. Int. J. Biol. Markers 16 (2), 112–120.
Da Pieve, C., Perkins, A.C., Missailidis, S., 2009. Nucl. Med. Biol. 36 (6), 703–710.
Damborský, P., Švitel, J., Katrlík, J., 2016. Essays Biochem. 60 (1), 91–100.
Darmostuk, M., Rimpelova, S., Gbelcova, H., Ruml, T., 2015. Biotechnol. Adv. 33 (6), 1141–1161.
Dehghani, S., Nosrati, R., Yousefi, M., Nezami, A., Soltani, F., Taghdisi, S.M., Abnous, K., Alibolandi, M., Ramezani, M., 2018. Biosens. Bioelectron. 110, 23–37.
Devine, P.L., McGuckin, M.A., Quin, R.J., Ward, B.G., 1994. Tumour Biol.: J. Int. Soc. Oncodev. Biol. Med. 15 (6), 337–344.
Devine, P.L., McGuckin, M.A., Ramm, L.E., Ward, B.G., Pee, D., Long, S., 1993. Cancer 72 (6), 2007–2015.
Dey, D., Goswami, T., 2011. J. Biomed. Biotechnol. 2011, 348218.
Ding, Y., Ling, J., Wang, H., Zou, J., Wang, K., Xiao, X., Yang, M., 2015. Anal. Methods 7 (18), 7792–7798.
do Carmo, F.S., Ricci-Junior, E., Cerqueira-Coutinho, C., de Souza Albernaz, M., Bernardes, E.S., Missailidis, S., Santos-Oliveira, R., 2017. Int J. Nanomed. 12, 53.
Eivazzadeh-Keihan, R., Pashazadeh-Panahi, P., Baradaran, B., Maleki, A., Hejazi, M., Mokhtarzadeh, A., de la Guardia, M., 2018. Trends Anal. Chem. 100, 103–115.
Eivazzadeh-Keihan, R., Pashazadeh, P., Hejazi, M., de la Guardia, M., Mokhtarzadeh, A., 2017. Trends Anal. Chem. 87, 112–128.
Fan, X., White, I.M., Shopova, S.I., Zhu, H., Suter, J.D., Sun, Y., 2008. Anal. Chim. Acta 620 (1–2), 8–26.
Farzin, L., Sadjadi, S., Shamsipur, M., Chabok, A., Sheibani, S., 2017. J. Electroanal. Chem. 807, 108–118.
Feng, J., Wu, X., Ma, W., Kuang, H., Xu, L., Xu, C., 2015. Chem. Commun. 51 (79), 14761–14763.
Ferreira, C., Matthews, C., Missailidis, S., 2006. Tumor Biol. 27 (6), 289–301.
Ferreira, C.S., Cheung, M.C., Missailidis, S., Bisland, S., Gariepy, J., 2008a. Nucleic Acids Res. 37 (3), 866–876.
Ferreira, C.S., Papamichael, K., Guilbault, G., Schwarzacher, T., Gariepy, J., Missailidis, S., 2008b. Anal. Bioanal. Chem. 390 (4), 1039–1050.
Florea, A., Ravalli, A., Cristea, C., Săndulescu, R., Marrazza, G., 2015. Electroanalysis 27 (7), 1594–1601.
Florea, A., Taleat, Z., Cristea, C., Mazloum-Ardakani, M., Săndulescu, R., 2013. Electrochem. Commun. 33, 127–130.
Frenette, P.S., Thirlwell, M.P., Trudeau, M., Thomson, D.M., Joseph, L., Shuster, J.S., 1994. Tumour Biol.: J. Int. Soc. Oncodev. Biol. Med. 15 (5), 247–254.
Gheybi, E., Amani, J., Salmanian, A.H., Mashayekhi, F., Khodi, S., 2014. Tumor Biol. 35 (11), 11489–11497.
Golichenari, B., Nosrati, R., Farokhi-Fard, A., Abnous, K., Vaziri, F., Behravan, J., 2018. Biosens. Bioelectron. 117, 319–331.
Gopinath, S.C.B., Lakshmipriya, T., Chen, Y., Phang, W.-M., Hashim, U., 2016. Biotechnol. Adv. 34 (3), 198–208.
Guo, P., Xiong, J., Zheng, D., Zhang, W., Liu, L., Wang, S., Gu, H., 2015. RSC Adv. 5 (81), 66355–66359.
Gupta, P., Bharti, A., Kaur, N., Singh, S., Prabhakar, N., 2018. J. Electroanal. Chem. 813, 102–108.
Hasanzadeh, M., Karimzadeh, A., Sadeghi, S., Mokhtarzadeh, A., Shadjou, N., Jouyban, A., 2016. J. Mater. Sci. Mater. Electron. 27 (6), 6488–6495.
Hasanzadeh, M., Razmi, N., Mokhtarzadeh, A., Shadjou, N., Mahboob, S., 2018. Int. J. Biol. Macromol. 108, 69–80.
He, L., Duan, F., Song, Y., Guo, C., Zhao, H., Tian, J.Y., Zhang, Z., Liu, C.S., Zhang, X., Wang, P., Du, M., Fang, S.M., 2017. 2D Mater. 4 (2).
He, Y., Lin, Y., Tang, H., Pang, D., 2012. Nanoscale 4 (6), 2054–2059.
Homola, J., Yee, S.S., Gauglitz, G., 1999. Sens. Actuators B: Chem. 54 (1), 3–15.
Hötzer, B., Medintz, I.L., Hildebrandt, N., 2012. Small 8 (15), 2297–2326.
Hu, R., Wen, W., Wang, Q., Xiong, H., Zhang, X., Gu, H., Wang, S., 2014. Biosens. Bioelectron. 53, 384–389.
Hu, S.W., Qiao, S., Pan, J.B., Kang, B., Xu, J.J., Chen, H.Y., 2018. Talanta 179, 9–14.
Hu, Y., Duan, J., Zhan, Q., Wang, F., Lu, X., Yang, X.-D., 2012. PLoS One 7 (2), e31970.
Huang, J., Luo, X., Lee, I., Hu, Y., Cui, X.T., Yun, M., 2011. Biosens. Bioelectron. 30 (1), 306–309.
Huang, R.-C., Chiu, W.-J., Lai, I.P.-J., Huang, C.-C., 2015. Sci. Rep. 5, 10292.
Hutter, E., Maysinger, D., 2013. Trends Pharmacol. Sci. 34 (9), 497–507.
Jia, S., Li, P., Koh, K., Chen, H., 2016. Mikrochim. Acta 183 (2), 683–688.
Jiang, X., Wang, H., Wang, H., Yuan, R., Chai, Y., 2016. Anal. Chem. 88 (18), 9243–9250.
Jiang, X., Wang, H., Wang, H., Zhuo, Y., Yuan, R., Chai, Y., 2017. Anal. Chem. 89 (7), 4280–4286.
Jo, H., Her, J., Ban, C., 2015. Biosens. Bioelectron. 71, 129–136.
Jonckheere, N., Van Seuningen, I., 2010. Biochimie 92 (1), 1–11.
Kang, W.J., Lee, J., Lee, Y.S., Cho, S., Ali, B.A., Al-Khedhairy, A.A., Heo, H., Kim, S., 2015. Colloids Surf. B: Biointerfaces 136, 134–140.
Karpik, A.E., Crulhas, B.P., Rodrigues, C.B., Castro, G.R., Pedrosa, V.A., 2017. Electroanalysis 29 (10), 2246–2253.
Keefe, A.D., Pai, S., Ellington, A., 2010. Nat. Rev. Drug Discov. 9 (7), 537.
Kong, R.M., Zhang, X.B., Chen, Z., Tan, W., 2011. Small 7 (17), 2428–2436.
Kulmala, S., Suomi, J., 2003. Anal. Chim. Acta 500 (1), 21–69.
Lakshmanan, I., Ponnusamy, M.P., Macha, M.A., Haridas, D., Majhi, P.D., Kaur, S., Jain, M., Batra, S.K., Ganti, A.K., 2015. J. Thorac. Oncol. 10 (1), 19–27.
Li, C., Meng, Y., Wang, S., Qian, M., Wang, J., Lu, W., Huang, R., 2015. ACS Nano 9 (12), 12096–12103.
Li, Q., Liu, L., Liu, J.-W., Jiang, J.-H., Yu, R.-Q., Chu, X., 2014. TrAC Trends Anal. Chem. 58, 130–144.
Li, S.K., Chen, A.Y., Niu, X.X., Liu, Z.T., Du, M., Chai, Y.Q., Yuan, R., Zhuo, Y., 2017a. Chem. Commun. 53 (69), 9624–9627.
Li, S.K., Liu, Z.T., Li, J.Y., Chen, A.Y., Chai, Y.Q., Yuan, R., Zhuo, Y., 2018. ACS Appl. Mater. Interfaces 10 (17), 14483–14490.
Li, T., Fan, Q., Liu, T., Zhu, X., Zhao, J., Li, G., 2010. Biosens. Bioelectron. 25 (12), 2686–2689.
Li, T., Yang, J., Ali, Z., Wang, Z., Mou, X., He, N., Wang, Z., 2017b. Sci. China Chem. 60 (3), 370–376.
Li, Y., Zhang, Y., Zhao, M., Zhou, Q., Wang, L., Wang, H., Wang, X., Zhan, L., 2016. Chem. Commun. 52 (20), 3959–3961.
Li, Z., Zhou, Y., Yan, D., Wei, M., 2017c. J. Mater. Chem. C 5 (14), 3473–3479.
Lin, C., Zheng, H., Huang, Y., Chen, Z., Luo, F., Wang, J., Guo, L., Qiu, B., Lin, Z., Yang, H., 2018. Biosens. Bioelectron. 117, 474–479.
Liu, C., Liu, X., Qin, Y., Deng, C., Xiang, J., 2016. RSC Adv. 6 (63), 58469–58476.
Liu, M., Yu, X., Chen, Z., Yang, T., Yang, D., Liu, Q., Du, K., Li, B., Wang, Z., Li, S., 2017. J. Nanobiotechnol. 15 (1), 81.
Liu, S., Xu, N., Tan, C., Fang, W., Tan, Y., Jiang, Y., 2018. Anal. Chim. Acta 1018, 86–93.
Liu, X., Qin, Y., Deng, C., Xiang, J., Li, Y., 2015. Talanta 132, 150–154.
Ma, C., Liu, H., Zhang, L., Li, H., Yan, M., Song, X., Yu, J., 2018. Biosens. Bioelectron. 99, 8–13.
Ma, F., Ho, C., Cheng, A.K., Yu, H.-Z., 2013. Electrochim. Acta 110, 139–145.
Marin, F., Luquet, G., Marie, B., Medakovic, D., 2007. Curr. Top. Dev. Biol. 80, 209–276.
Meirinho, S.G., Dias, L.G., Peres, A.M., Rodrigues, L.R., 2016. Biotechnol. Adv. 34 (5), 941–953.
Mir, T.A., Yoon, J.-H., Gurudatt, N., Won, M.-S., Shim, Y.-B., 2015. Biosens. Bioelectron. 74, 594–600.
Missailidis, S., Thomaidou, D., Borbas, K.E., Price, M.R., 2005. J. Immunol. Methods 296 (1), 45–62.
Miyazaki, C.M., Shimizu, F.M., Ferreira, M., 2017. 6 - surface plasmon resonance (SPR) for sensors and biosensors. In: Da Róz, A.L., Ferreira, M., de Lima Leite, F., Oliveira, O.N. (Eds.), Nanocharacterization Techniques. William Andrew Publishing, pp. 183–200.
Mokhtarzadeh, A., Tabarzad, M., Ranjbari, J., de la Guardia, M., Hejazi, M., Ramezani, M., 2016. Trends Anal. Chem. 82, 316–327.
Moreno, M., Bontkes, H.J., Scheper, R.J., Kenemans, P., Verheijen, R.H.M., von Mensdorff-Pouilly, S., 2007. Cancer Lett. 257 (1), 47–55.
Nabavinia, M.S., Gholoobi, A., Charbgoo, F., Nabavinia, M., Ramezani, M., Abnous, K., 2017. Med. Res. Rev. 37 (6), 1518–1539.
Nath, S., Mukherjee, P., 2014. Trends Mol. Med. 20 (6), 332–342.
Nosrati, R., Dehghani, S., Karimi, B., Yousefi, M., Taghdisi, S.M., Abnous, K., Alibolandi, M., Ramezani, M., 2018. Biosens. Bioelectron. 117, 1–14.
Ogasawara, D., Hachiya, N.S., Kaneko, K., Sode, K., Ikebukuro, K., 2009. Biosens. Bioelectron. 24 (5), 1372–1376.
Oguzhan Caglayan, M., 2017. Curr. Anal. Chem. 13 (1), 18–30.
Phillips, J.A., Lopez-Colon, D., Zhu, Z., Xu, Y., Tan, W., 2008. Anal. Chim. Acta 621 (2), 101–108.
Pickup, J.C., Hussain, F., Evans, N.D., Rolinski, O.J., Birch, D.J.S., 2005. Biosens. Bioelectron. 20 (12), 2555–2565.
Ping, J., Zhou, Y., Wu, Y., Papper, V., Boujday, S., Marks, R.S., Steele, T.W.J., 2015. Biosens. Bioelectron. 64, 373–385.
Qi, C., Cai, S., Wang, X., Li, J., Lian, Z., Sun, S., Yang, R., Wang, C., 2016. RSC Adv. 6 (60), 54949–54955.
Qu, A., Wu, X., Xu, L., Liu, L., Ma, W., Kuang, H., Xu, C., 2017. Nanoscale 9 (11), 3865–3872.
Radom, F., Jurek, P.M., Mazurek, M.P., Otlewski, J., Jeleń, F., 2013. Biotechnol. Adv. 31 (8), 1260–1274.
Rahn, J.J., Dabbagh, L., Pasdar, M., Hugh, J.C., 2001. Cancer.: Interdiscip. Int. J. Am. Cancer. Soc. 91 (11), 1973–1982.
Robertson, J.F.R., Pearson, D., Price, M.R., Selby, C., Badley, R.A., Pearson, J., Blamey, R.W., Howell, A., 1990. Eur. J. Cancer Clin. Oncol. 26 (11), 1127–1132.
Roda, A., Mirasoli, M., Michelini, E., Di Fusco, M., Zangheri, M., Cevenini, L., Roda, B., Simoni, P., 2016. Biosens. Bioelectron. 76, 164–179.
Roy, L.D., Sahraei, M., Subramani, D.B., Besmer, D., Nath, S., Tinder, T.L., Bajaj, E., Shanmugam, K., Lee, Y.Y., Hwang, S.I., 2011. Oncogene 30 (12), 1449.
Rughetti, A., Fama, A., von Mensdorff-Pouilly, S., Taurino, F., Rahimi, H., Ribersani, M., Natalino, F., D'Elia, G., Bizzoni, L., Latagliata, R., 2008. Circulating MUC1 levels (CA15. 3) in myeloproliferative disorders (MPD). Am. Soc. Hematol.
Seo, H.B., Gu, M.B., 2017. J. Biol. Eng. 11 (1), 11.
Sharma, B., Frontiera, R.R., Henry, A.-I., Ringe, E., Van Duyne, R.P., 2012. Mater. Today 15 (1), 16–25.
Siegel, R.L., Miller, K.D., Jemal, A., 2015. CA: Cancer J. Clin. 65 (1), 5–29.
Singh, R., Bandyopadhyay, D., 2007. Cancer Biol. Ther. 6 (4), 481–486.
Song, J., Zhou, Y., Chen, B., Lou, W., Gu, J., 2017. Int. J. Electrochem. Sci. 12 (6), 5618–5627.
Song, S., Wang, L., Li, J., Fan, C., Zhao, J., 2008. TrAC Trends Anal. Chem. 27 (2), 108–117.
Song, Y., Wei, W., Qu, X., 2011. Adv. Mater. 23 (37), 4215–4236.
Su, L., Jia, W., Hou, C., Lei, Y., 2011. Biosens. Bioelectron. 26 (5), 1788–1799.
Sun, Y., Liu, Y., Vernier, P., Liang, C., Chong, S., Marcu, L., Gundersen, M., 2006. Nanotechnology 17 (17), 4469.

Taleat, Z., Cristea, C., Marrazza, G., Mazloum-Ardakani, M., Săndulescu, R., 2014. J. Electroanal. Chem. 717, 119–124.
Tian, J., Huang, T., Lu, J., 2016. Anal. Methods 8 (11), 2375–2382.
Turner, A.P., 2013. Chem. Soc. Rev. 42 (8), 3184–3196.
Valeur, B., Berberan-Santos, M.N., 2012. Molecular Fluorescence: Principles and Applications. John Wiley & Sons.
Vigneshvar, S., Sudhakumari, C.C., Senthilkumaran, B., Prakash, H., 2016. Front. Bioeng. Biotechnol. 4, 11.
Wang, B., Akiba, U., Anzai, J.-I., 2017a. Molecules 22 (7), 1048.
Wang, K., He, M.Q., Zhai, F.H., He, R.H., Yu, Y.L., 2017b. Talanta 166, 87–92.
Wang, M., Hu, B., Ji, H., Song, Y., Liu, J., Peng, D., He, L., Zhang, Z., 2017c. ACS Omega 2 (10), 6809–6818.
Wang, Z., Xia, N., Shi, J., Li, S., Zhao, Y., Wang, H., Liu, L., 2014. Anal. Lett. 47 (14), 2431–2442.
Wang, Z., Yu, J., Gui, R., Jin, H., Xia, Y., 2016. Biosens. Bioelectron. 79, 136–149.
Wei, W., Pan, X., Li, D., Qian, J., Yin, L., Pu, Y., Liu, S., 2012. J. Nanosci. Nanotechnol. 12 (10), 7685–7691.
Wen, W., Hu, R., Bao, T., Zhang, X., Wang, S., 2015. Biosens. Bioelectron. 71, 13–17.
Wijaya, E., Lenaerts, C., Maricot, S., Hastanin, J., Habraken, S., Vilcot, J.-P., Boukherroub, R., Szunerits, S., 2011. Curr. Opin. Solid State Mater. Sci. 15 (5), 208–224.
Wilson, G.S., Gifford, R., 2005. Biosens. Bioelectron. 20 (12), 2388–2403.
Wu, M.S., Yuan, D.J., Xu, J.J., Chen, H.Y., 2013. Anal. Chem. 85 (24), 11960–11965.
Xiang, J., Pi, X., Chen, X., Xiang, L., Yang, M., Ren, H., Shen, X., Qi, N., Deng, C., 2017. Biosens. Bioelectron. 96, 268–274.
Xu, H., Kou, F., Ye, H., Wang, Z., Huang, S., Liu, X., Zhu, X., Lin, Z., Chen, G., 2017. Talanta 175, 177–182.
Yan, M., Sun, G., Liu, F., Lu, J., Yu, J., Song, X., 2013. Anal. Chim. Acta 798, 33–39.
Yang, D., Liu, M., Xu, J., Yang, C., Wang, X., Lou, Y., He, N., Wang, Z., 2018a. Talanta 185, 113–117.
Yang, F., Jiang, X., Zhong, X., Wei, S., Yuan, R., 2018b. Sens. Actuator B-Chem. 265, 126–133.
Yazdian-Robati, R., Arab, A., Ramezani, M., Langroodi, F.A., Abnous, K., Taghdisi, S.M., 2016. Biosens. Bioelectron. 82 (Suppl. C), S162–S172.
Zhang, C., Ji, X., Zhang, Y., Zhou, G., Ke, X., Wang, H., Tinnefeld, P., He, Z., 2013. Anal. Chem. 85 (12), 5843–5849.
Zhang, J.J., Cheng, F.F., Zheng, T.T., Zhu, J.J., 2017. Biosens. Bioelectron. 89, 937–945.
Zhang, N., Li, W., Guo, Z., Sha, Y., Wang, S., Su, X., Jiang, X., 2016. Electroanalysis 28 (7), 1504–1509.
Zhang, Y., Guo, S., Huang, H., Mao, G., Ji, X., He, Z., 2018. Anal. Chim. Acta.
Zhao, B., Wu, P., Zhang, H., Cai, C., 2015. Biosens. Bioelectron. 68, 763–770.
Zhao, J., He, X., Bo, B., Liu, X., Yin, Y., Li, G., 2012. Biosens. Bioelectron. 34 (1), 249–252.
Zhao, X., Zhang, M., Wei, D., Wang, Y., Yan, S., Liu, M., Yang, X., Yang, K., Cui, H.L., Fu, W., 2017. Biomed. Opt. Express 8 (10), 4427–4437.
Zhou, B., Qiu, Y., Wen, Q., Zhu, M., Yang, P., 2017. ACS Appl. Mater. Interfaces 9 (3), 2074–2082.
Zhu, C., Yang, G., Li, H., Du, D., Lin, Y., 2014. Anal. Chem. 87 (1), 230–249.
Zhu, X., Kou, F., Xu, H., Lin, L., Yang, G., Lin, Z., 2017. Sens. Actuator B-Chem. 253, 660–665.
Zhu, X., Yang, J., Liu, M., Wu, Y., Shen, Z., Li, G., 2013. Anal. Chim. Acta 764, 59–63.